Quantum Monte Carlo investigations of density functional theory of the strongly inhomogeneous electron gas

Maziar Nekovee
Complexity Research Group, Polaris 134, BT Exact, Martlesham, Suffolk IP5 3RE, UK

W. M. C. Foulkes*
The Blackett Laboratory, Imperial College London, Prince Consort Road, London SW7 2AZ, UK

R. J. Needs
Cavendish Laboratory, Madingley Road, Cambridge CB3 0HE, UK
(Dated: October 5, 2002)

We use a variational quantum Monte Carlo realization of the adiabatic connection technique to calculate the most relevant quantities in Hohenberg-Kohn-Sham density functional theory for several strongly inhomogeneous electron gas systems. Results for the coupling-constant dependence of the exchange-correlation energy, the pair-correlation function, the exchange-correlation hole, and the exchange and correlation energy densities are presented. Comparisons are made with the interaction strength interpolation (ISI) approximation, the local density approximation (LDA), the gradient expansion approximation (GEA), the generalized gradient approximation (GGA), and the weighted density approximation (WDA). The coupling-constant dependence of the exchange-correlation energy is accurately described by an ISI model that incorporates information on the strong interaction limit. Unlike either the LDA or the GEA, the WDA is successful in describing the non-local structure of the exchange-correlation hole. The LDA errors in the exchange-correlation energy density show a remarkable correlation with the Laplacian of the density. The GGA worsens the error in the integrated exchange-correlation energy as the inhomogeneity of the systems increases. This failure is shared by current meta-GGA functionals, and is shown to be caused by the inability of these functionals to describe the LDA overestimation (in absolute value) of the exchange energy density around density maxima. It is suggested that this effect could be taken into account by including Laplacian terms in semilocal density functionals.

PACS numbers: 71.15.Mb, 71.10.-w, 71.45.Gm

I. INTRODUCTION

Given any system of interacting electrons, density functional theory[1,2] (DFT) shows that there exists a functional $E[n]$ of the electron density $n(\mathbf{r})$ that is minimized and equal to the ground-state energy when $n(\mathbf{r})$ is equal to the ground-state density. In the Kohn-Sham formulation,[3] these striking results are turned into a computational scheme by mapping the many-electron system onto a fictitious system of non-interacting electrons moving in an effective one-electron potential that produces the density $n(\mathbf{r})$. The only contribution to $E[n]$ that cannot be calculated exactly within this approach is the exchange-correlation energy, $E_{xc}[n]$, which is known to be a universal and unique functional of $n(\mathbf{r})$. The exchange-correlation functional provides the link between the ground-state energy of the real many-electron system and that of the Kohn-Sham electrons, and its functional derivative $v_{xc}(\mathbf{r}) = \delta E_{xc}/\delta n(\mathbf{r})$ is part of the effective potential through which these fictitious electrons move. The core problem in the application of DFT is to find increasingly accurate and yet computationally tractable approximations to the unknown functional $E_{xc}[n]$.

The local density approximation[3] (LDA) is obtained by writing

$$E_{xc}[n] = \int d\mathbf{r}\, e_{xc}([n], \mathbf{r}) \tag{1}$$

and assuming that $e_{xc}([n], \mathbf{r})$, the exchange-correlation energy density at the point $\mathbf{r}$, is the same as in a homogeneous electron gas with uniform density $n = n(\mathbf{r})$. The LDA has proved to be far more accurate than expected *a priori* and its computational simplicity has made it possible to obtain accurate estimates for the ground-state energies and structural properties of many solids. However, applications to surface chemistry, quantum chemistry, and computational biology require the calculation of total energies to a precision at least an order of magnitude better than the LDA can provide.

Many attempts have been made to develop approximate exchange-correlation functionals that are more accurate than the LDA. These efforts fall into three main categories.[2] In the so-called semilocal approaches, one allows $e_{xc}([n], \mathbf{r})$ to depend on the electron density at the point $\mathbf{r}$, as in the LDA, plus various gradients of the electron density at $\mathbf{r}$. In the fully nonlocal approaches, an approximation for $e_{xc}([n], \mathbf{r})$ is sought by modeling the exchange-correlation hole $n_{xc}(\mathbf{r}, \mathbf{r}')$ or the pair-correlation function $g_{xc}(\mathbf{r}, \mathbf{r}')$ near $\mathbf{r}$. Finally, a number of authors have attempted to approximate

the coupling-constant dependence of E_{xc}. The generalized gradient approximation[4–7] (GGA) and extensions thereof[8] fall into the first category; the average density approximation[9] and the weighted density approximation[9] belong to the second category; and the so-called hybrid schemes[10] are in the last category.

Although better than the LDA in many situations, current GGAs are not able to improve upon the LDA consistently. Moreover, despite much effort spent in optimizing their parameters, they seem unable to achieve the very high accuracy of ∼0.1 eV required to study, e.g., the majority of interesting chemical reactions. Most of the fully nonlocal approaches were formulated before the appearance of the GGA, but they proved difficult to implement and unable to match the accuracy of the GGA consistently. The use of nonlocal functionals is now computationally practical, however, and this has led to a renewal of interest.

The quest for improved approximations to $E_{xc}[n]$ is the subject of much current research. Several directions are being investigated, but progress has been hampered by the lack of highly accurate results for the key quantities in density functional theory, E_{xc}, n_{xc}, g_{xc} and e_{xc}, in systems with strong density inhomogeneities. Such data is needed to provide points of reference and for testing new functionals. The integrated exchange-correlation energies of such systems can be obtained from accurate many-body calculations of the ground state using, e.g., the configuration interaction (CI) method in atoms and molecules or quantum Monte Carlo methods in extended systems. The exchange-correlation energy delivered by an approximate functional is not, however, the ultimate probe of its quality; the total exchange-correlation energy is obtained by integrating the exchange-correlation energy density over the system, and a very accurate E_{xc} could be obtained from an erroneous e_{xc} because of fortuitous error cancellations. A more stringent test is provided by a point-by-point comparison between the forms of n_{xc} and e_{xc} assumed in the density functional and the results of high-quality many-body calculations. Unfortunately, evaluating n_{xc} and e_{xc} requires performing the computationally demanding coupling-constant integration that appears in the adiabatic connection formula (see below), and few such results are available at present.

In the adiabatic connection, an exact expression is obtained for E_{xc} by scaling the electron-electron interaction by a factor λ and varying λ between 0 and 1, while keeping the electron density fixed at the ground-state density $n(\mathbf{r})$ of the fully interacting ($\lambda = 1$) system. The exchange-correlation energy density (per electron) at point $\mathbf{r}$ is then expressed as the electrostatic interaction between the reference electron at $\mathbf{r}$ and its λ-averaged exchange-correlation hole: $n_{xc}(\mathbf{r}, \mathbf{r}') = \int d\lambda\, n^{\lambda}_{xc}(\mathbf{r}, \mathbf{r}')$. In many-body wavefunction approaches such as quantum Monte Carlo (QMC) and CI, n^{λ}_{xc} is obtained directly from the ground-state many-body wavefunction Ψ^{λ} of the Hamiltonian associated with λ.[11] However, this Hamiltonian contains an a-priori unknown λ-dependent potential V^{λ} which ensures that the electron density is fixed at $n(\mathbf{r})$ as λ varies. The presence of this unknown potential renders adiabatic connection calculations computationally more complex and expensive than conventional ground-state calculations, since in principle both Ψ^{λ} and V^{λ} need to be determined self-consistently. In atoms and small molecules, CI calculations can be adapted to perform the adiabatic connection procedure. A few such calculations have been carried out for two and four electron systems,[12,13] but CI calculations are not feasible in extended systems because of their unfavorable scaling with the number of electrons.

The state-of-the-art computational approach to the ground-state many-body problem of extended systems is the quantum Monte Carlo method, which comes in two versions. The (essentially) exact but computationally rather expensive fixed-node diffusion Monte Carlo (DMC) method, and the less accurate but computationally more affordable variational Monte Carlo (VMC) method. In DMC, the analogy between the imaginary-time many-electron Schrödinger equation and a diffusion plus branching equation is used to sample the exact ground-state many-body wavefunction via a random walk in the configuration space of the electrons.[14] The VMC method is based on an explicitly parameterized trial ground-state wavefunction. Expectation values are evaluated by the Metropolis Monte Carlo technique,[14] and the parameters in the trial wavefunction are varied in order to minimize either the energy expectation value or the fluctuations of the local energy.[14,15] The quality of any VMC calculation depends on the choice of the trial wavefunction, but previous work has shown that most VMC calculations for extended systems recover $85-95\%$ of the correlation energy.[15]

As discussed above, realization of the adiabatic connection procedure requires self-consistent computation of both Ψ^{λ} and the unknown potential V^{λ} for a range of values of λ. Performing self-consistent DMC calculations for strongly inhomogeneous systems is currently beyond reach because of the high computational cost and the difficulty in formulating self-consistent DMC. Recently, however, we devised a VMC-based methodology for realizing the adiabatic connection procedure. Our approach is based on a constrained variance reduction procedure that provides V^{λ} whilst simultaneously optimizing the trial many-body wavefunction Ψ^{λ}, followed by Monte Carlo Metropolis integration of the multi-dimensional integrals involved in the evaluation of n^{λ}_{x} and e^{λ}_{xc}.[16]

In this paper, we use our methodology to calculate n_{xc}, g_{xc}, e_{xc}, and the λ-dependence of E_{xc} for three different electron gas systems with strong, roughly sinusoidal, density modulations in one direction. A brief summary of our findings has already been published.[17] Preliminary results for one of our systems were also discussed in Ref. 16, although these had rather large systematic and finite-size errors. Here we present new results and analysis, along with a more complete description of our methodology.

The rest of this paper is organized as follows. In Sec. II we outline the adiabatic connection approach used to obtain the forms of n_{xc} and e_{xc} relevant in DFT. We also review our computational scheme for realizing the adiabatic connection within variational quantum Monte Carlo. Sec. III describes the systems studied and the details of the computations carried out. In Sec. IV we present and analyze our results for the adiabatic curves, pair-correlation functions, and exchange-correlation holes. This is followed by an analysis of the performance of the LDA and the GGA in describing exchange-correlation energy densities, considering exchange and correlation contributions separately. Sec. V concludes this paper.

II. METHODOLOGY

A. The adiabatic connection

Consider a system of N interacting electrons in the presence of an external potential. In the Hohenberg-Kohn-Sham formulation of DFT, the ground-state energy of this system is the minimum value of the total energy functional

$$E[n] = T_s[n] + \int d\mathbf{r}\, V_{\rm ext}(\mathbf{r}) n(\mathbf{r}) + E_H[n] + E_{xc}[n] \; . \quad (2)$$

Here $T_s[n]$ is the kinetic energy of a fictitious non-interacting system of N electrons having the same electron density, $n(\mathbf{r})$, as the interacting system, $V_{\rm ext}(\mathbf{r})$ is the externally applied one-electron potential, and

$$E_H[n] = \frac{1}{2} \int d\mathbf{r} \int d\mathbf{r}' \frac{n(\mathbf{r}) n(\mathbf{r}')}{|\mathbf{r} - \mathbf{r}'|} \quad (3)$$

is the Hartree (electrostatic) energy. (Note that Hartree atomic units are used throughout this paper: charges are measured in units of the fundamental charge e, masses in units of the electron mass m, distances in Bohr radii, and energies in Hartrees, where 1 Hartree = 2 Rydbergs $\approx$ 27.2 eV.) The exchange-correlation energy functional $E_{xc}[n]$ is usually defined by Eq. (2) and contains all the many-body contributions not included in the other terms.

An exact expression[18] for $E_{xc}[n]$ may be obtained by scaling the electron-electron interaction by a factor λ and varying λ between 1 (the real system) and 0 (a non-interacting system), whilst simultaneously adjusting the external potential to keep the electron density equal to $n(\mathbf{r})$. The exchange-correlation functional is then given by

$$E_{xc}[n] = \int_0^1 d\lambda \, W_{xc}^{\lambda}[n] \; , \quad (4)$$

where

$$W_{xc}^{\lambda}[n] = \langle \Psi^{\lambda} | \hat{V}_{ee} | \Psi^{\lambda} \rangle - E_H[n] \; , \quad (5)$$

and Ψ^{λ} is the antisymmetric ground state of the Hamiltonian

$$\hat{H}^{\lambda} = \hat{T} + \lambda \hat{V}_{ee} + \hat{V}^{\lambda} \quad (6)$$

associated with coupling constant λ. Here $\hat{T}$ and $\hat{V}_{ee}$ are the operators for the kinetic and electron-electron interaction energies, and $\hat{V}^{\lambda} = \sum_i V^{\lambda}(\mathbf{r}_i)$ is the one-electron potential needed to hold the electron density $n^{\lambda}(\mathbf{r})$ associated with Ψ^{λ} equal to $n(\mathbf{r})$ for all values of λ between 0 and 1.

The expectation value from Eq. (5) may be rewritten as

$$\langle \Psi^{\lambda} | \hat{V}_{ee} | \Psi^{\lambda} \rangle = \frac{1}{2} \int d\mathbf{r} \int d\mathbf{r}' \, \frac{n^{\lambda}(\mathbf{r}, \mathbf{r}')}{|\mathbf{r} - \mathbf{r}'|} \; , \quad (7)$$

where

$$n^{\lambda}(\mathbf{r}, \mathbf{r}') = \langle \Psi^{\lambda} | \sum_i^N \sum_{j \, (\neq i)}^N \delta(\mathbf{r} - \mathbf{r}_i) \delta(\mathbf{r}' - \mathbf{r}_j) | \Psi^{\lambda} \rangle \quad (8)$$

is the diagonal part of the two-particle density matrix at coupling constant λ. The exchange-correlation hole at coupling constant λ is defined via

$$n^{\lambda}(\mathbf{r}, \mathbf{r}') = n(\mathbf{r}) n(\mathbf{r}') + n(\mathbf{r}) n_{xc}^{\lambda}(\mathbf{r}, \mathbf{r}') \; , \quad (9)$$

and hence

$$E_{xc}[n] = \frac{1}{2} \int d\mathbf{r} \int d\mathbf{r}' \, \frac{n(\mathbf{r}) n_{xc}(\mathbf{r}, \mathbf{r}')}{|\mathbf{r} - \mathbf{r}'|} \; , \quad (10)$$

where

$$n_{xc}(\mathbf{r}, \mathbf{r}') = \int_0^1 d\lambda \, n_{xc}^{\lambda}(\mathbf{r}, \mathbf{r}') \quad (11)$$

is the coupling-constant-averaged exchange-correlation hole.[18]

Eq. (10) may be written as

$$E_{xc}[n] = \int d\mathbf{r} \; e_{xc}([n], \mathbf{r}) \; , \quad (12)$$

where

$$e_{xc}([n], \mathbf{r}) = \frac{1}{2} \int d\mathbf{r}' \, \frac{n(\mathbf{r}) n_{xc}(\mathbf{r}, \mathbf{r}')}{|\mathbf{r} - \mathbf{r}'|} \quad (13)$$

is the exchange-correlation energy density derived from the adiabatic connection procedure. Expressing the energy density as a coupling-constant integral,

$$e_{xc}([n], \mathbf{r}) = \int_0^1 d\lambda \; e_{xc}^{\lambda}([n], \mathbf{r}) \; , \quad (14)$$

we obtain

$$e_{xc}^{\lambda}([n], \mathbf{r}) \; = \; \langle \Psi_{\lambda} | \frac{1}{2} \sum_i^N \sum_{j \, (\neq i)}^N \frac{\delta(\mathbf{r} - \mathbf{r}_i)}{|\mathbf{r} - \mathbf{r}_j|} | \Psi_{\lambda} \rangle - \frac{1}{2} \int d\mathbf{r}' \, \frac{n(\mathbf{r}) n(\mathbf{r}')}{|\mathbf{r} - \mathbf{r}'|} \; . \quad (15)$$

For future reference, we note that $\Psi^{\lambda=0}$ is the Slater determinant of the exact Kohn-Sham orbitals corresponding to the density $n(\mathbf{r})$. Furthermore, $n_{xc}^{\lambda=0}$ is the exact *density-functional* exchange hole n_x corresponding to the density-functional exchange energy density $e_x = e_{xc}^{\lambda=0}$. The correlation energy density is defined by $e_c = e_{xc} - e_x$.

B. Quantum Monte Carlo realization

Given an interacting many-body system with ground-state density $n(\mathbf{r})$, the main ingredient required to evaluate n_{xc} and e_{xc} is the many-body wavefunction Ψ^λ at a range of different values of the coupling constant λ. Since Ψ^λ is an eigenfunction of $\hat{H}^\lambda$, it follows that the local energy

$$E_L^\lambda(\mathbf{R}) = \frac{\hat{H}^\lambda \Psi^\lambda(\mathbf{R})}{\Psi^\lambda(\mathbf{R})} \tag{16}$$

is equal to a constant, the eigenvalue E^λ, at all points $\mathbf{R} = (\mathbf{r}_1, \mathbf{r}_2, \ldots \mathbf{r}_N)$ in the $3N$-dimensional configuration space of electron coordinates. In conventional variational Monte Carlo calculations,[15] this property is used to find an overall fit to Ψ^λ using a variance-reduction technique.[14,19,20] The procedure is to determine the parameters $\{\alpha\}$ in the trial function $\Psi_T^\lambda(\mathbf{R}, \{\alpha\})$ by minimizing the variance σ^2 of the local energy:

$$\sigma^2 = \int d\mathbf{R} \left[\frac{\hat{H}^\lambda \Psi_T^\lambda(\mathbf{R})}{\Psi_T^\lambda(\mathbf{R})} - E[\Psi_T^\lambda] \right]^2 |\Psi_T^\lambda(\mathbf{R})|^2 , \tag{17}$$

where $E[\Psi_T^\lambda]$ is the expectation value of $\hat{H}^\lambda$ with wavefunction Ψ_T^λ.

The above optimization cannot be applied to the case of coupling-constant integration because the Hamiltonian contains the unknown potential $\hat{V}^\lambda = \sum_i V^\lambda(\mathbf{r}_i)$. In their pioneering VMC study of bulk silicon,[21] Hood *et al.* circumvented this problem by using an LDA approximation for $V^\lambda(\mathbf{r})$. This works well in systems where the LDA effective potential is accurate (such as Si), but might be problematic in other situations. Our approach[16] has been to introduce a trial potential $V_T^\lambda(\mathbf{r})$ and to treat *both* $\Psi_T^\lambda(\mathbf{R})$ and $V_T^\lambda(\mathbf{r})$ variationally, determining the variational parameters by simultaneously minimizing the variance of the local energy *and* the error in the density $n_T^\lambda(\mathbf{r})$ obtained from $\Psi_T^\lambda(\mathbf{R})$. This is achieved by expanding both $n_T^\lambda(\mathbf{r})$ and the target density $n(\mathbf{r})$ in a flexible orthonormal set of N_d basis functions and defining a modified penalty function,

$$\mu^2 = \sigma^2 + W \sum_{s=1}^{N_d} \left[n_s - n_{T,s}^\lambda \right]^2 , \tag{18}$$

where W is a weighting factor, the magnitude of which determines the emphasis laid on the fixed-density constraint, and n_s and $n_{T,s}^\lambda$ are the expansion coefficients of $n(\mathbf{r})$ and $n_T(\mathbf{r})$, respectively. The above penalty function reaches its lower bound of zero if and only if: (i) Ψ_T^λ is the exact many-body wavefunction Ψ_λ satisfying the fixed-density constraint (within the accuracy set by N_d); and (ii) V_T^λ is the corresponding exact potential V^λ. Hence, minimization of μ^2 will in principle result in the *simultaneous* determination of Ψ^λ and V^λ. In practice, the constrained search is restricted to a subset of potentials and many-body wavefunctions, and minimization of μ^2 yields an approximate potential V^λ and wavefunction Ψ^λ.

Our numerical implementation of the above scheme works as follows. We start with initial guesses for Ψ_T^λ and V_T^λ. A set of statistically independent configurations $\{\mathbf{R}_i : i = 1, \ldots, M\}$ (we used $M \sim 10000$) is then sampled from $|\Psi_T^\lambda \mathbf{R})|^2$ using the Metropolis algorithm. Next, the Monte Carlo estimators of σ^2 and the expansion coefficients $n_{T,s}^\lambda$ are evaluated, enabling the current value of the penalty function μ^2 to be obtained. The variational parameters in Ψ_T^λ and V_T^λ are then modified[22] and the estimators recalculated (over the same set of configurations) until μ^2 is minimized. For each value of λ, this procedure is repeated several times until the variational coefficients reach convergence. Once the optimal Ψ_T^λ has been obtained, we evaluate n_{xc}^λ and e_{xc}^λ with a set of long VMC runs. Finally, e_{xc} and n_{xc} are obtained by performing the coupling-constant integration using 6 equally spaced values of λ between 0 and 1 inclusive.[23]

III. SYSTEM AND COMPUTATIONAL DETAILS

A. Systems

All calculations carried out were for spin-unpolarized electron gases in finite face-centered-cubic simulation cells subject to periodic boundary conditions. The exact interacting ground-state density $n(\mathbf{r})$ was chosen *a priori*, and the constrained minimization scheme was then used to find, at each λ, the exact (within VMC) wavefunction Ψ^λ and external potential V^λ corresponding to that density. At full coupling (λ=1), when $V^\lambda(\mathbf{r})$ is the exact external potential of the many-electron system with ground-state density $n(\mathbf{r})$, this procedure might be viewed as a VMC realization of Hohenberg and Kohn's first theorem:[1] given the exact ground-state density, we find the corresponding ground-state many-body wavefunction and external potential.

The input densities $n(\mathbf{r})$ were generated by solving, within the LDA, the Kohn-Sham equations for an external potential of the form $V_q \cos(\mathbf{q}.\mathbf{r})$, where V_q was fixed at $2.08\epsilon_F^0$ and ϵ_F^0 is the Fermi energy corresponding to the average density $n^0 = 3/4\pi r_s^3$. The advantages of this approach are that the input electron density is guaranteed to be noninteracting v-representable and that the Slater determinant of single-particle orbitals is by construction the exact many-body wavefunction cor-

responding to λ=0. The (density-functional) exchange contributions to e_{xc}, n_{xc}, and E_{xc} obtained from this Slater determinant are therefore also exact.[16]

The three simulation cells studied had all the same average electron density $n^0 = 3/(4\pi r_s^3)$, where $r_s = 2$ a.u. (roughly the same as for aluminum), but slightly different numbers of electrons: $N = 64$, 78, and 68 (and hence slightly different volumes). The wave vector $\mathbf{q}$ of the cosine potential in each simulation cell was aligned with the third of the three symmetry-equivalent primitive reciprocal lattice vectors, $\mathbf{B}_1$, $\mathbf{B}_2$, and $\mathbf{B}_3$ of the cells, and was set at $\mathbf{q} = n\mathbf{B}_3$, $n = 2, 3, 4$, respectively. The resulting magnitudes of these wavevectors (to four digit accuracy) are $1.1080k_F^0$, $1.557k_F^0$, and $2.172k_F^0$, respectively, with $k_F^0 = (3\pi^2 n^0)^{1/3}$. The reason for choosing slightly different numbers of electrons for these systems was to ensure that the highest occupied shell of degenerate LDA orbitals corresponding to each system was always completely occupied; this is common practice in quantum Monte Carlo calculations for extended systems and helps to mitigate finite-size effects. As $\mathbf{q}$ varies, the structure of the LDA energy spectrum changes and it is necessary to change the number of electrons to satisfy this condition.

B. Many-body wavefunctions and interaction Hamiltonian

We used the following Slater-Jastrow form[15] for Ψ_T^λ:

$$\Psi_T^\lambda = D^\uparrow D^\downarrow \exp\left[-\sum_{i>j} u^\lambda_{\sigma_i,\sigma_j}(r_{ij}) + \sum_i \chi^\lambda(\mathbf{r}_i)\right] , \quad (19)$$

where $r_{ij} = |\mathbf{r}_i - \mathbf{r}_j|$ and $D^\uparrow$ and $D^\downarrow$ are Slater determinants of spin-up and spin-down exact Kohn-Sham orbitals corresponding to density $n(\mathbf{r})$, with $\Psi_T^{\lambda=0} = D^\uparrow D^\downarrow$. The two-body functions $u^\lambda_{\sigma_i,\sigma_j}$, which depend on the spins σ_i and σ_j of the electrons involved, correlate the motion of pairs of electrons. For simplicity, it is assumed that $u^\lambda_{\sigma_i,\sigma_j}$ is a function of the inter-electronic distance r_{ij} only, as would be the case in a uniform system. This is less than ideal, but previous work[24] has shown that the resulting errors are extremely small in the systems of interest here (despite the fact that these systems are strongly inhomogeneous). The one-body functions χ^λ, which are absent in the homogeneous electron gas, are crucial for a satisfactory description of systems with inhomogeneity.[24,25]

Following Williamson *et al.*,[20] we set

$$u^\lambda(r) = u_0^\lambda(r) + f^\lambda(r) , \quad (20)$$

where $u_0^\lambda(r)$ is a fixed function described below and $f^\lambda(r)$ is optimized variationally. The variational part f^λ is equal to

$$B^\lambda(\frac{L_{WS}}{2} + r)(L_{WS} - r)^2 + r^2(L_{WS} - r)^2 \sum_{n=0}^{N_T} \alpha_n^\lambda T_n(\overline{r}) \quad (21)$$

if $r \le L_{WS}$ or zero otherwise. Here B^λ and α_n^λ are adjustable parameters, T_n is the n^{th} Chebyshev polynomial, N_T is an integer constant (in our case $N_T = 9$), and

$$\overline{r} = \frac{2r - L_{WS}}{L_{WS}} . \quad (22)$$

In the last two equations, L_{WS} is the radius of the sphere centered on the origin that just touches the Wigner-Seitz cell of the simulation cell.

At full coupling ($\lambda = 1$), the fixed part of u^λ takes the short-ranged Yukawa form,[20]

$$u_0^1(r) = \frac{A^1}{r}\left(1 - e^{-r/F^1}\right) e^{-r^2/L_0^2} , \quad (23)$$

where $A^1 = 1/\omega_p^0$ is related to the plasma frequency $\omega_p^0 = \sqrt{4\pi n^0}$ of a uniform electron gas of density n^0. The cusp conditions[14,15] then imply that $F^1_{\sigma_i,\sigma_j} = \sqrt{2A^1}$ for parallel spins and $F^1_{\sigma_i,\sigma_j} = \sqrt{A^1}$ for anti-parallel spins. The remaining parameter, L_0, is set equal to $0.25L_{WS}$, ensuring that $u_0(L_{WS})$ is practically zero.

To determine u_0^λ for other values of λ, we note that a scaling argument (see Appendix A) shows that the wavefunction $\Psi^\lambda_{r_s}$ of a uniform electron gas with coupling constant λ and density parameter r_s may be obtained from the wavefunction $\Psi^{\lambda=1}_{r_s'}$ of a uniform electron gas with coupling constant $\lambda = 1$ and density parameter $r_s' = \lambda r_s$ as follows:

$$\Psi^\lambda_{r_s}(\mathbf{r}_1, \mathbf{r}_2, \ldots \mathbf{r}_N) = C^\lambda \Psi^{\lambda=1}_{r_s'}(\lambda\mathbf{r}_1, \lambda\mathbf{r}_2, \ldots \lambda\mathbf{r}_N) , \quad (24)$$

where C^λ is a normalization constant. If we impose this condition on the Slater-Jastrow wavefunction of a uniform electron gas (for which, of course, $\chi = 0$), we obtain

$$u_0^\lambda(r) = \frac{A^\lambda}{r}\left(1 - e^{-r/F^\lambda}\right) e^{-r^2/L_0^2} , \quad (25)$$

where $A^\lambda = \lambda^{1/2} A^1$ and $F^\lambda = \lambda^{-1/4} F^1$. Since the u functions used in this work are homogeneous, it is reasonable to insist that they too satisfy this scaling relation. We note that with the above choice for A^λ and F^λ, the λ-dependent cusp conditions[14] are automatically satisfied.

The electron-electron interaction Hamiltonian used in these simulations has the form:[26]

$$\hat{H}_{ee} = \sum_{i>j} v_{\text{MI}}(\mathbf{r}_i - \mathbf{r}_j) + \sum_i \int d\mathbf{r}\, n(\mathbf{r}) \left[\frac{1}{|\mathbf{r}_i - \mathbf{r}|} - v_{\text{MI}}(\mathbf{r}_i - \mathbf{r})\right] , \quad (26)$$

where $v_{\text{MI}}(\mathbf{r})$ is a minimum-image-truncated Coulomb interaction, equal to $1/r$ if $\mathbf{r}$ is inside the Wigner-Seitz cell of the simulation cell or zero otherwise. This interaction results in smaller Coulomb finite-size effects than the standard Ewald interaction when finite simulation cells and periodic boundary conditions are used to simulate

infinitely extended systems.[26] In most calculations, the ground-state density $n(\mathbf{r})$ appearing in the above equation has to be obtained self-consistently (in practice it normally suffices to use the LDA density). In the present work, however, since the ground-state density is defined *a priori*, no self-consistency loop is required.

C. Calculation details

The electron density is modulated only in the $\mathbf{B}_3$ direction, and hence both the one-body part of the Jastrow factor χ^λ and the effective potential V^λ may be expanded as one-dimensional Fourier series:

$$\chi^\lambda(\mathbf{r}) = \sum_{m=1}^{M} \chi_m^\lambda \cos(m\mathbf{B_3}.\mathbf{r}) \ , \tag{27}$$

$$V^\lambda(\mathbf{r}) = \sum_{m=1}^{M} V_m^\lambda \cos(m\mathbf{B}_3.\mathbf{r}) \ . \tag{28}$$

The electron density is expanded in a similar way (with the inclusion of the $m = 0$ term). The one-dimensional nature of the inhomogeneity also greatly reduces the number of Fourier coefficients needed to represent the diagonal part of the density matrix:

$$n^\lambda(\mathbf{r},\mathbf{r}') = \sum_{\substack{\mathbf{K}_\parallel \\ m,m'}} n^\lambda_{\mathbf{K}_\parallel,m,m'} \, e^{i\mathbf{K}_\parallel\cdot(\mathbf{r}-\mathbf{r}')} \, e^{im\mathbf{B}_3\cdot\mathbf{r}} \, e^{im'\mathbf{B}_3\cdot\mathbf{r}'} \ , \tag{29}$$

where $\mathbf{K}_\parallel = n_1\mathbf{B}_1 + n_2\mathbf{B}_2$ and n_1 and n_2 are integers. A similar representation is used for $n^\lambda_{xc}(\mathbf{r},\mathbf{r}')$.

At each λ, we used a total of 20 variational parameters in u^λ and up to 7 coefficients in the plane-wave expansions of χ^λ and V^λ. The cut-offs in the Fourier expansions of $n^\lambda(\mathbf{r},\mathbf{r}')$ and $n^\lambda_{xc}(\mathbf{r},\mathbf{r}')$ were increased until a satisfactory description of the zero coupling ($\lambda = 0$) exact exchange results, as obtained from the Slater determinant of Kohn-Sham orbitals, was achieved.

The optimization of the parameters in Ψ^λ and V^λ was performed using 96000 statistically uncorrelated electron configurations. This was sufficient to reduce the root mean square deviation of $n^\lambda(\mathbf{r})$ from $n(\mathbf{r})$ to less than 0.5% of $n(\mathbf{r})$ for all values of λ and all systems. The expectation values were calculated using 10^6 independent configurations of all electrons.

D. Analysis of statistical, finite-size and systematic errors

There are three sources of error in our calculations: (i) statistical errors; (ii) finite-size errors caused by the fact that we are modeling a supposedly infinite system by a simulation cell containing a finite number of electrons; and (iii) VMC errors, which result from the approximate nature of Ψ^λ.

With 10^6 configurations used in sampling all physical quantities, we found statistical errors to be negligible except in the tails of the exchange-correlation holes and pair-correlation functions in the low density regions of our systems. By evaluating the exchange hole both directly and by Monte Carlo sampling, and assuming that the errors in n_{xc} for $\lambda \neq 0$ were similar to those for $\lambda = 0$, we verified that these errors were much smaller that the differences between n_{xc} and n^{LDA}_{xc}.

The remaining errors are caused by the finite size of the system and the approximate nature of Ψ^λ. The use of the minimum-image-truncated interaction instead of the standard Ewald interaction greatly reduces finite-size errors in e_x. However, the remaining finite-size and systematic errors combine such that, even in a homogeneous electron gas, $e^{VMC}_{xc} \neq e^{LDA}_{xc}$.

In order to estimate and mitigate these errors, we performed additional VMC calculations of the exchange and correlation energies of finite homogeneous electron gases with $N = 64$ and $r_s = 0.8$, 1, 2, 3, 4, 5, 8, and 10. This enabled us to construct a Perdew-Zunger parameterization[27] of the VMC exchange-correlation energy per electron of a finite uniform electron gas with $N = 64$. By comparing this VMC-based finite-size parameterization with the exact results for the homogeneous electron gas, we were able to obtain local density estimates of the systematic errors in e_x and e_c. These estimates showed that the finite-size errors in e_x (which are the only errors because e_x is obtained from the exact Kohn-Sham orbitals) are no more than 0.5% of this quantity, while the combined finite-size and systematic errors in e_c are ∼15% of this quantity. The above errors in e_x are typically less than 5% of the calculated energy density differences $e^{LDA}_x - e_x$ while the above errors in e_c are less than 30% of $e^{LDA}_c - e_c$. To further reduce the remaining errors in these differences, we used our finite-size VMC parameterization as input for the evaluation of e^{LDA}_c and e^{LDA}_x. This parameterization was also used in the evaluation of the total LDA and GGA[4] exchange and correlation energies, a procedure that we assume mitigates the errors in $E^{LDA}_{xc} - E^{VMC}_{xc}$ and $E^{GGA}_{xc} - E^{VMC}_{xc}$.

IV. RESULTS

A. Adiabatic curves

The formal properties and coupling-constant dependence of the integrand $W^\lambda_{xc}[n]$ from Eq. (4) have been the subject of several numerical and analytical studies. Hood *et al.*[21] evaluated $W^\lambda_{xc}[n]$ for bulk silicon using the variational Monte Carlo method. Joubert and Srivastava[12] and Colonna and Savin[13] calculated $E^\lambda_{xc}[n]$, the exchange-correlation energy associated with λ, for several two and four electron systems and a range of values of λ between 0 and 2. Görling and Levy[28] and Savin[29] developed a perturbation expansion of the corre-

lation contribution to this quantity,

$$W_c^\lambda[n] = W_{xc}^\lambda[n] - E_x[n] \ , \tag{30}$$

around $\lambda = 0$. Ernzerhof[30] developed models for the change in the λ-dependence of E_{xc}^λ in molecules upon atomization, making use of information on the exact E_x and the generalized gradient approximation to E_{xc}. Finally, the limiting behavior of $W_{xc}^\lambda[n]$ as $\lambda \to \infty$ was investigated in a series of papers by Perdew and coworkers.[31–33] Some of the key properties that are known exactly are:

$$W_{xc}^{\lambda=0}[n] = E_x[n] < 0 \ , \tag{31}$$

$$\frac{dW_{xc}^\lambda[n]}{d\lambda} < 0 \quad (\lambda \geq 0) \ , \tag{32}$$

$$\lim_{\lambda\to\infty} W_{xc}^\lambda[n] = W_{xc}^\infty[n] \quad \text{is finite.} \tag{33}$$

In Fig. 1 we display our VMC results for W_c^λ (per electron) as a function of λ. It can be seen that W_c^λ decreases smoothly and monotonically as λ increases, in agreement with theoretical predictions and previous numerical calculations. In order to obtain further insight into the behavior of this quantity, we fitted our data to the quadratic form

$$W_c^{\lambda,q} = a\lambda + b\lambda^2 \ , \tag{34}$$

and the Padé form

$$W_c^{\lambda,p} = -\alpha\frac{\beta\lambda^2 + 2\lambda}{(1+\beta\lambda)^2} \ , \tag{35}$$

which were examined in Ref. 12, and to the Yukawa form,

$$W_c^{\lambda,y} = c\left(\frac{1-\exp(-d\lambda)}{\lambda} - d\right) \ . \tag{36}$$

The resulting fits are displayed in Fig. 1. It can be seen that all three forms provide a good description of our data in the range $0 \leq \lambda \leq 1$. We found, however, that the Padé and Yukawa forms produce the smallest root-mean-square errors. Furthermore, the quadratic form is only reasonable over a finite range of λ, while both the Padé and Yukawa forms yield fits for W_{xc}^λ that satisfy Eqs. (32–33) and are reasonable for $0 \leq \lambda \leq \infty$. The rather good fit of our data to a quadratic indicates that any interpolation scheme that gives the correct value (i.e., zero) and derivative of W_c^λ at $\lambda = 0$ and the correct value at one other point in the range $0 < \lambda \leq 1$ should work well in our systems.[34]

The asymptotic behavior of W_{xc}^λ in the limit $\lambda \to \infty$ has been a subject of considerable interest. Just as the so-called hybrid schemes[10] make use of information about $W_{xc}^{\lambda=1}$ in the construction of approximations for $W_{xc}^{0\leq\lambda\leq1}$, it has been suggested that information about $W_{xc}^{\lambda\to\infty}$ may be used to boost the accuracy of approximate functionals. Recently, Seidl, Perdew, and Kurth[33] proposed the following interaction-strength interpolation model (ISI) for W_{xc}^λ:

$$W_{xc}^{\lambda,ISI} = W_{xc}^\infty + \frac{X}{\sqrt{1+\lambda Y}+Z} \ , \tag{37}$$

where

$$X = \frac{xy^2}{z^2} \ , \quad Y = \frac{x^2y^2}{z^4} \ , \quad Z = \frac{xy^2}{z^3} - 1 \ ,$$

$$x = -2W_{xc}^{\prime,0} \ , \quad y = W_{xc}^{\prime,\infty} \ , \quad z = W_{xc}^0 - W_{xc}^\infty \ ,$$

and the primes denote derivatives with respect to λ. Combining the ISI model with the point-charge-plus-continuum (PC) approximation[32] for W_{xc}^∞ and $W_{xc}^{\prime,\infty}$, these authors arrived at a new correlation functional[33] that incorporates information only on the weak coupling ($\lambda = 0$) and strong coupling ($\lambda = \infty$) limits. The PC approximations are:

$$W_{xc}^{\infty,PC} = \int d\mathbf{r}\left[An(\mathbf{r})^{4/3} + B\frac{|\nabla n(\mathbf{r})|^2}{n(\mathbf{r})^{4/3}}\right] \tag{38}$$

and

$$W_{xc}^{\prime,\infty,PC} = \int d\mathbf{r}\left[Cn(\mathbf{r})^{3/2} + D\frac{|\nabla n(\mathbf{r})|^2}{n(\mathbf{r})^{7/6}}\right] \ , \tag{39}$$

where A, B, C and D are constants.[32] In both the above expressions, the first term is a local density approximation and the second a gradient correction.

In the ISI model, the derivative $W_{xc}^{\prime,0}$ is obtained using Görling-Levy perturbation theory[28] around $\lambda = 0$ and is expressed in terms of the occupied and unoccupied Kohn-Sham orbitals. Here, however, in order to examine the accuracy of the PC part of the ISI-PC approximation, we computed $W_{xc}^{\prime,0}$ directly from the above fits (both the Padé and the Yukawa forms were used, resulting in slightly different values for $W_{xc}^{\prime,0}$). The PC approximation was then used to compute W_{xc}^∞ and $W_{xc}^{\prime,\infty}$. Figure 2 shows the resulting curves for $W_c^{\lambda,ISI} = W_{xc}^{\lambda,ISI} - E_x$ in the $q = 1.556k_F^0$ system over the range $0 < \lambda \leq 2$. Also shown are our VMC results (for $0 \leq \lambda \leq 1$). It can be seen that the ISI-PC model describes our VMC data with great accuracy, a success that is repeated in the other two systems. The ISI-PC correlation energies are also very accurate, underestimating (in absolute value) the VMC correlation energies by less than 2%. This is in line with previous findings regarding the performance of the ISI model in atoms and two-electron systems,[33] although we note that a more consistent comparison of the ISI-PC model with our VMC results would require evaluating $W_{xc}^{\prime,0}$ directly from the Görling-Levy expression. The agreement between the ISI-PC model and our results become less satisfactory if the gradient terms in Eqs. (38–39) are omitted, as can be seen in Fig. 2. This indicates that the inclusion of these terms is important for the success of the ISI-PC model in our systems.

Before closing this subsection, we make some observation regarding the analytic behavior of W_c^λ at $\lambda = 0$. In a three-dimensional homogeneous electron gas, W_c^λ is known to have an infinite slope at $\lambda = 0$, but the slope is finite in atoms and in the infinitely extended two-dimensional electron gas.[33] The above fits to our VMC data indicate that W_c^λ has a finite slope in our systems as well. These results suggest that the analytical behavior of W_c^λ at $\lambda = 0$ is system dependent, and is possibly determined by the analytical structure (as a function of energy) of the single-particle Green's function associated with the Kohn-Sham electrons.

B. Pair-correlation functions and exchange-correlation holes

The exchange-correlation hole is a key quantity in DFT and provides a simple visualization of the electronic correlations in inhomogeneous systems. The explicit relation between n_{xc} and E_{xc} has also provided the impetus behind many of the proposed corrections to the LDA. The average density approximation[9] (ADA) and weighted density approximation[9] (WDA) make explicit use of this relation to construct nonlocal approximate density functionals. The GGAs most popular in solid state applications[4,5] have as their starting point the gradient expansion of n_{xc} for a weakly inhomogeneous electron gas.

The exchange-correlation hole $n_{xc}(\mathbf{r}, \mathbf{r}')$ is the average over the coupling constant of the change in electron density at $\mathbf{r}'$ caused by the presence of an electron at $\mathbf{r}$ (by definition, this density change excludes the delta function corresponding to the electron at $\mathbf{r}$ itself). When there is an electron at $\mathbf{r}$ there must be one fewer electron in the rest of the system, and hence the exchange-correlation hole satisfies the sum rule

$$\int d\mathbf{r}' \; n_{xc}(\mathbf{r}, \mathbf{r}') = -1 \; . \tag{40}$$

The exchange part of n_{xc} satisfies the above sum rule as well as the negativity condition[18]

$$n_x(\mathbf{r}, \mathbf{r}') \leq 0 \; . \tag{41}$$

The density-functional pair-correlation function $g_{xc}(\mathbf{r}, \mathbf{r}')$ is related to n_{xc} through the following equation:

$$n_{xc}(\mathbf{r}, \mathbf{r}') = n(\mathbf{r}')[g_{xc}(\mathbf{r}, \mathbf{r}') - 1] \; . \tag{42}$$

In physical terms, the pair-correlation function is the coupling-constant average of the probability of finding an electron at point $\mathbf{r}'$ provided there is one at point $\mathbf{r}$, divided by the probability of finding an electron at $\mathbf{r}'$ without this constraint. The pair-correlation function satisfies several conditions, including

$$g_{xc}(\mathbf{r}, \mathbf{r}') \geq 0 \; , \tag{43}$$

and

$$\lim_{|\mathbf{r}-\mathbf{r}'|\to\infty} g_{xc}(\mathbf{r}, \mathbf{r}') = 1 \; . \tag{44}$$

The LDA exchange-correlation hole is given by

$$n_{xc}^{LDA}(\mathbf{r}, \mathbf{r}') = n(\mathbf{r})[g_{xc}^h(|\mathbf{r}' - \mathbf{r}|, n(\mathbf{r})) - 1] \; , \tag{45}$$

where $g_{xc}^h(|\mathbf{r}' - \mathbf{r}|, n)$ is the pair-correlation function of a uniform electron gas with density n.

To provide a detailed visualization of the behavior of the exchange-correlation hole and pair-correlation function in a strongly inhomogeneous system, we produced an animation showing g_{xc}^{VMC} and n_{xc}^{VMC} around an electron that moves in the $q = 1.1080 k_F^0$ simulation cell along a line parallel to $\mathbf{q}$ (the direction of maximum inhomogeneity) from a density maximum to the neighboring density minimum. Since this system resembles a periodic array of thin metallic slabs separated by vacuum gaps, our results are relevant to understanding the behavior of n_{xc} and g_{xc} at and in the vicinity of metallic surfaces. Figure 3 shows snapshots of the animation for g_{xc}. The pair-correlation function is displayed as a function of $\mathbf{r}'$ around a fixed electron at $\mathbf{r}$, with $\mathbf{r}'$ ranging in a plane parallel to $\mathbf{q}$. Also shown are the corresponding LDA pair-correlation function, g_{xc}^{LDA}, and a schematic electron density profile.

The LDA pair-correlation function is spherically symmetric around the electron and its spatial extent is controlled by the local Fermi wave vector $k_F(\mathbf{r})^{-1} = (3\pi^2 n(\mathbf{r}))^{-1/3}$. This is in sharp contrast to the behavior observed in our VMC simulations. At the density maximum (top panel), g_{xc}^{VMC} is strongly anisotropic and greatly elongated in the direction of the inhomogeneity. In fact, g_{xc}^{VMC} extends almost twice as far in the direction of the inhomogeneity as in the perpendicular direction. As the electron moves away from the density maximum to a point on the slope (middle panel), g_{xc}^{VMC} maintains its box-like shape but becomes asymmetric, bulging out in the direction of increasing electron density. Consequently, the most important contributions to the exchange-correlation hole at this point come from the high density regions on one side of the probe electron. At the density minimum, both the VMC and LDA pair-correlation functions have very large spatial extents. However, unlike g_{xc}^{LDA}, which extends isotropically in all directions, g_{xc}^{VMC} is more extended in the direction of the density inhomogeneity than in the perpendicular direction. Given the similarity of our system to a stack of metallic slabs, we would expect the pair-correlation function of an electron sitting in the vacuum region between two such slabs to show a similar channel-like shape. Thus, our results may be relevant to understanding the origin of the image potential, which results from long-ranged correlation outside metal surfaces.

The stretching of the pair-correlation function in the direction of the inhomogeneity, and its asymmetric shape in regions of high density gradient, were also seen in the other two systems we considered. Clearly, such behavior cannot be modeled by a spherically symmetric Ansatz

for g_{xc}, as is attempted in the construction of the ADA and WDA functionals.[9] Although such effects may be less pronounced when the density varies strongly in all directions, they should be observable in systems such as surfaces,[35] quasi-two-dimensional electron gases,[36] and the Airy gas,[37] all of which have strong one-dimensional density modulations.

We now turn to our results for the exchange-correlation hole. These were discussed briefly in Ref. 17 but are further analyzed here in the light of our findings for g_{xc}^{VMC}. We refer the reader to Fig. 1 of Ref. 17 for snapshots of the hole in the $q = 1.1080k_F^0$ system. At the density maximum, both n_{xc}^{VMC} and n_{xc}^{LDA} are centered on the electron. However, unlike n_{xc}^{LDA}, which is always spherically symmetric, n_{xc}^{VMC} is contracted in the direction of the inhomogeneity. As the electron moves away from the density maximum to a point on the slope, the nonlocal nature of n_{xc}^{VMC} becomes manifest. While n_{xc}^{LDA} is still centered on the electron and is rather diffuse, n_{xc}^{VMC} lags behind near the density maximum and is much more compact. This nonlocality occurs because of the extension of the pair-correlation function in the direction of increasing density, which encompasses the density maximum. The nonlocal behavior of n_{xc}^{VMC} becomes remarkable at the density minimum. Here n_{xc}^{VMC} has two strong minima, each centered at a density maximum. The LDA hole, by contrast, is spread over the whole system in order to satisfy the exchange-correlation sum rule, Eq. (40). Once again, the nonlocal behavior of n_{xc}^{VMC} is a consequence of the extension of the pair-correlation function in the direction of the inhomogeneity, which now encompasses two density maxima. The LDA pair-correlation function is also very long-ranged at this point, but since the LDA exchange-correlation hole is obtained by multiplying the LDA pair-correlation function by $n(\mathbf{r})$ instead of $n(\mathbf{r}')$, the LDA hole is not strongly enhanced around the density maxima.

Very recently, Rushton *et al.*[38] used our VMC results[17] to investigate the performance of the WDA in three strongly inhomogeneous systems with density distributions very close to those studied here. The nonlocality of n_{xc}^{WDA} at density minima, the behavior of e_{xc}^{WDA}, and the resulting trends in E_{xc}^{WDA}, were all found to be very similar to the results described above. This indicates that fully non-local WDA functionals are capable of providing accurate description of n_{xc} in some strongly inhomogeneous systems.

It is also of interest to examine whether semilocal functionals are able to capture some of the structure of n_{xc}. Since semilocal models for the λ-averaged correlation hole are not currently available, we focus here on examining semilocal models of n_x. The exchange hole n_x may be expressed in terms of the Kohn-Sham orbitals and is thus a functional of the electron density. By performing a second-order gradient expansion of this functional,[39] Perdew[40] derived a gradient expansion approximation (GEA), $n_x^{GEA}(\mathbf{r}' - \mathbf{r}, n(\mathbf{r}), \nabla n(\mathbf{r}), \nabla_i \nabla_j n(\mathbf{r}))$, of the exchange hole. To impose the conditions expressed in Eqs. (40–41), which are not obeyed by the GEA hole, Perdew then applied a real-space cutoff. The result was a "meta-GGA" hole, n_x^{MGGA}, that contained both first and second derivatives of the electron density. Subsequently, Perdew and Wang[5] derived a GGA model for the exchange hole by integrating the expression for E_x^{GEA} in terms of n_x^{GEA} by parts, thus eliminating the second-order derivative terms, and then cutting off the resulting hole in real space. Thus, while the GEA hole and the meta-GGA hole are directly comparable with the exact n_x, the integration by parts invalidates any direct comparison with n_x^{GGA}. We chose to compare our results with a GEA hole that had the unphysical positive tail removed. The additional real-space cutoff required to obtain the meta-GGA hole was not applied, but this does not affect the qualitative behavior discussed below.

Energetically, the most significant points in our systems are near the density maxima. In Fig. 4 we have plotted the exact exchange hole for the $q = 1.1080k_F^0$ system around a probe electron at a density maximum. At this point, n_x is centered at the probe electron, just like n_x^{LDA}, but is contracted in the direction of the inhomogeneity. This behavior becomes more pronounced in the two other systems we studied, and should also be observable in quasi-two-dimensional electron gases. By construction, the LDA is unable to describe any deformation of the hole from a spherically symmetric shape. The truncated GEA hole is non-spherical at this point, but is extended rather than contracted in the direction of the inhomogeneity.

In Fig. 5 we have plotted the exact exchange hole for the $q = 1.1080k_F^0$ system around a probe electron at a density minimum. Also shown are the corresponding LDA and truncated GEA holes. At this point, n_x shows a strongly nonlocal behavior similar to that observed previously[17] for n_{xc}, having two large nonlocal minima at the adjacent density maxima. Neither n_x^{LDA} nor n_x^{GEA} is capable of capturing this behavior. The LDA hole is spread over the whole system and has its minimum value at the position of the probe elctron. The GEA hole, on the other hand, has a saddle point precisely at the position of the probe electron, and large spurious positive tails further out (which have been truncated as explained above). We note that the exact, LDA and GEA holes all satisfy $n_x(r, r) = -n(r)/2$, i.e., the value of the so-called ontop exchange hole is fixed by the electron density at that point.

The above results show that the meta-GGA functional form is unable to describe the structure of the exchange hole in strongly inhomogeneous systems such as ours, despite the fact that it makes use of both the gradient and the Laplacian of the electron density. We note also that the resulting meta-GGA exchange energy density depends linearly on the Laplacian of the electron density while our previous results[17] indicated a non-linear dependence of e_x on this quantity in our systems.

C. Exchange-correlation energy densities

We now turn to our results for exchange-correlation energy densities. The LDA for the exchange-correlation energy of a spin-unpolarized system is

$$E_{xc}^{LDA}[n] = \int d\mathbf{r}\; n(\mathbf{r})\, \epsilon_{xc}^{\rm unif}(n(\mathbf{r}))\;, \qquad (46)$$

where $\epsilon_{xc}^{\rm unif}(n(\mathbf{r}))$ is the exchange-correlation energy per particle of a uniform electron gas with density $n = n(\mathbf{r})$. The GGA incorporates information on the density gradient at $\mathbf{r}$ as follows:

$$E_{xc}^{GGA}[n] = \int d\mathbf{r}\; n(\mathbf{r})\, \epsilon_{xc}^{\rm unif}(n(\mathbf{r}))\, F_{xc}^{GGA}(s(\mathbf{r}))\;, \qquad (47)$$

where $F_{xc}^{GGA}(s)$ is the GGA enhancement factor and

$$s(\mathbf{r}) = \frac{|\nabla n(\mathbf{r})|}{2k_F(\mathbf{r})n(\mathbf{r})} \qquad (48)$$

is a dimensionless density gradient. By analogy with Eq. (12), one may define a GGA exchange-correlation energy density e_{xc}^{GGA} as

$$e_{xc}^{GGA}([n],\mathbf{r}) = n(\mathbf{r})\, \epsilon_{xc}^{\rm unif}(n(\mathbf{r}))\, F_{xc}^{GGA}(s(\mathbf{r}))\;. \qquad (49)$$

In general, however, since only the integral of $e_{xc}([n],\mathbf{r})$ is defined uniquely, the above quantity need not correspond directly to the exchange-correlation energy density calculated from the coupling-constant integral, Eq. (14). For example, as discussed in the previous subsection, the GGA for exchange introduced by Perdew and coworkers[4,5] is obtained by cutting off the spurious long-ranged part of the second-order gradient expansion of an exchange hole derived from n_x^{GEA} by performing an integration by parts. The integration alters the exchange energy density and thus invalidates any comparison with the exchange energy density derived directly from n_x

Figure 6 shows $e_{xc}^{LDA}([n],\mathbf{r}) - e_{xc}^{VMC}([n],\mathbf{r})$ for the $q = 2.172k_F^0$ system. Results for the two other systems can be seen in Fig. 3 of Ref. 17. Here and in the following paragraphs, $e_{xc}^{LDA}([n],\mathbf{r})$ is calculated using the exact ground-state density $n(\mathbf{r})$. The results are plotted along a line parallel to $\mathbf{q}$ (we call this direction y). Also shown are $n(\mathbf{r})$ and $\nabla^2 n(\mathbf{r})$ plotted along the same line. As mentioned above, e_{xc}^{GGA} does not correspond to the e_{xc} obtained from the coupling-constant integration. Nevertheless, we consider it interesting to display the difference $e_{xc}^{GGA} - e_{xc}^{VMC}$ on the same plot.

It is apparent that the shape, magnitude, and sign of the LDA errors in e_{xc} closely follow the shape, magnitude, and sign of $\nabla^2 n(\mathbf{r})$. The LDA errors in e_{xc} are large and negative in regions where $\nabla^2 n(\mathbf{r})$ is large and negative (around density maxima), and large and positive in regions where $\nabla^2 n(\mathbf{r})$ is large and positive. This is a direct consequence of the fact that the LDA overestimates the depth and underestimates the size of the (spherically averaged) exchange-correlation hole in the regions around the density maxima in our systems, while it underestimates the depth and overestimates the size in the tail regions.[16] Similar behavior has been observed previously in the silicon atom[41] and in molecules.[42] In these systems, the negative LDA errors around the density maxima are overcompensated by positive errors in other regions, and the GGA corrections improve the LDA value of the total exchange-correlation energy E_{xc}. In our systems, by contrast, the LDA errors in E_{xc} change sign from positive (for the q=$1.11k_F^0$ system) to negative (for the two other systems) as q increases and the negative contributions to Δe_{xc}, which occur where $\nabla^2 n(\mathbf{r}) < 0$, become dominant.[17]

In the construction of approximate functionals, the exchange e_x and correlation e_c contributions to e_{xc} are often treated separately. Next we investigate the performance of the LDA for these quantities. (Preliminary results for the $q = 1.1080k_F^0$ system were discussed in Ref. 16. The treatment of finite-size and systematic errors has improved greatly since then, however, and the calculations reported here are at least an order of magnitude more accurate.) The differences $\Delta e_x = e_x^{LDA} - e_x^{VMC}$ and $\Delta e_c = e_c^{LDA} - e_c^{VMC}$ are shown in Fig. 7. It can be seen that $\Delta e_c \le 0$ everywhere and in all systems, and that the spatial variations in this quantity roughly follow the variations in the electron density. The exchange energy differences, Δe_x, show a more complicated structure and roughly follow the variations of the Laplacian of the density (although not as closely as does Δe_{xc}); they are positive in the tail regions but change sign and become negative around the density maxima. In the $q = 1.1080k_F^0$ system, Δe_x and Δe_c partially cancel each other, but this cancellation of errors becomes less effective as the electron density becomes more rapidly varying. In fact, in the two other systems, one can see a "conspiracy of errors" occurring around the density maxima.

To further investigate the performance of the LDA in these systems, we calculated the cumulative LDA errors in the exchange and correlation energy densities:

$$\Delta e_{x,c}^{LDA,{\rm cum}}(y) = \int_0^y dy_1\, \Delta e_{x,c}^{LDA}(y_1)\;. \qquad (50)$$

The results are shown in Fig. 8. For the $q = 1.1080k_F^0$ system, $\Delta e_x^{LDA,{\rm cum}}$ is positive everywhere, indicating that the positive LDA errors in the tail regions dominate. As q increases, however, the oscillations in $\Delta e_x^{LDA,{\rm cum}}$ become more pronounced and both positive and negative regions can be seen near $y = 0$. For the $q = 2.172k_F^0$ system, $\Delta e_x^{LDA,{\rm cum}}$ fluctuates between positive and negative values, resulting in an almost perfect cancellation of errors in the integrated E_x. By contrast, $\Delta e_c^{LDA,{\rm cum}}$ is always negative and does not change qualitatively as the electron density becomes more rapidly varying.

Our results for the total exchange energy are shown in Table I (results for E_{xc} can be found in Table I of Ref. 17), along with the differences ΔE_x^{LDA} and ΔE_x^{GGA}. These results reflect the behavior seen above for $\Delta e_x^{LDA,{\rm cum}}$ and

$\Delta e_c^{LDA,\mathrm{cum}}$: the error in the integrated exchange energy is largest in the $q = 1.1080k_F^0$ system and reduces almost to zero in the $q = 2.172k_F^0$ system because of the real-space cancellation of errors. The GGA corrections to E_x^{LDA} are by construction always negative; they improve the LDA value for the $q = 1.1080k_F^0$ system but worsen it for the two other systems.

D. Exchange enhancement factors

If the electron density has a convergent Taylor expansion about a point $\mathbf{r}$, a knowledge of n and all its gradients at $\mathbf{r}$ is sufficient to construct the electron density everywhere within the radius of convergence. If we assume that the radius of convergence is greater than the length scale of the electronic correlations, the exchange-correlation energy density $e_{xc}([n], \mathbf{r})$, which is a functional of the form of the electron density within that length scale, may be written as:

$$\begin{aligned} E_{xc}[n] &= \int d\mathbf{r}\; e_{xc}([n], \mathbf{r}) \\ &= \int d\mathbf{r}\; e_{xc}(n(\mathbf{r}), \nabla_i n(\mathbf{r}), \nabla_i \nabla_j n(\mathbf{r}), \ldots)\;, \end{aligned} \quad (51)$$

where e_{xc} is now a simple function (not a functional) of the density and all its derivatives at $\mathbf{r}$. In the case of the exchange energy, E_x, this expression may be combined (see Appendix B) with symmetry arguments and the scaling property,[43]

$$E_x[\gamma^3 n(\gamma\mathbf{r})] = \gamma E_x[n(\mathbf{r})] \qquad (\gamma > 0)\;, \quad (52)$$

to deduce that

$$E_x = \int d\mathbf{r}\; e_x(\mathbf{r}, [n]) = \int d\mathbf{r}\; e_x^{LDA}(n(\mathbf{r}))\, F_x(s, l, \ldots)\;, \quad (53)$$

where $s(\mathbf{r})$ is the dimensionless density gradient introduced in Eq. (48),

$$l(\mathbf{r}) = \frac{\nabla^2 n(\mathbf{r})}{4k_F^2(\mathbf{r}) n(\mathbf{r})} \quad (54)$$

is a dimensionless Laplacian, and F_x is the so-called exchange enhancement factor.

Semilocal approximations may be viewed as attempts to find energetically accurate "projections" of e_{xc} onto a finite space spanned by $n(\mathbf{r})$ and a few derivatives of n at $\mathbf{r}$. In the case of the GGA exchange functional, where only the first derivative is considered, F_x is approximated as a function of s only. This makes sense when all higher dimensionless derivatives of the density are small. In general, however, the exact F_x need not be a single-valued function of s alone: a strongly inhomogeneous system may contain many points with the same value of s but different values of F_x. Moreover, even when a single-valued representation is possible for one system, there is no guarantee that the same representation will work in other systems.

In atoms and a few other cases, the electron density profile is such that there is a one-to-one mapping from s to l and all higher order gradients: i.e., $l = l(s)$. The higher order gradients can therefore be eliminated and an exact single-variable enhancement factor, $\tilde{F}_x(s)$, defined, which may be accurately approximated using a GGA form. Such an enhancement factor will not in general be transferable to other systems, but its existence might explain why the GGA is so successful in atoms.

A step beyond the GGA would be to project F_x onto the space spanned by s and l. In order to see how well such a projection might work, we have calculated the exact exchange enhancement factor at many points on the y axes of each of our systems and plotted the results against the values of s and l at those points. The resulting scatter map of F_x against (s, l) is shown in Fig. 9. It can be seen that, for our systems, F_x appears to be a single-valued function of (s, l). However, any attempt to regard F_x as a function of s or l alone, equivalent to a projection of Fig. 9 onto either the (s, F_x) or the (l, F_x) plane, results in a loss of uniqueness (see also Fig. 3 in Ref. 17). In particular, if one tries to regard F_x as a function of s but not l, most values of s correspond to two very different values of F_x. This effect is especially striking near $s = 0$, where the exact F_x attains values both larger (exchange enhancement) and smaller (exchange de-enhancement) than unity. A projection onto the (l, F_x) plane is more successful in our systems and is able to describe both the exchange enhancement and the exchange de-enhancement near $s = 0$. In fact, for each individual system, there is a unique mapping from l to position and from there to all higher derivatives of the density. For any one system, it is therefore possible to obtain an exact representation of the enhancement factor that depends on l only. Unfortunately, the exact l-dependent enhancement factors obtained for the three different systems are not quite the same, showing that there is no "universally" accurate form (even in our very restricted sample space).

A recent extension of the GGA is the meta-GGA (MGGA) functional, in which the exchange enhancement factor is written as a function of the reduced density gradient, the Laplacian of the density, and the orbital kinetic energy density. Several versions of the MGGA have been suggested, but here we consider only the form introduced by Perdew, Kurth, Zupan, and Blaha (PKZB).[8] One feature of the PKZB MGGA exchange enhancement factor is that it is always greater than or equal to unity, implying that the PKZB MGGA exchange energy is always lower than the LDA exchange energy. This form of the MGGA therefore suffers from the same deficiency as the GGA in systems such as ours, where the exchange de-enhancement effect is important or dominant.

V. CONCLUSIONS AND OUTLOOK

We used a variational Monte Carlo realization of the adiabatic connection method to investigate the central quantities appearing in Hohenberg-Kohn-Sham density-functional theory for three strongly inhomogeneous electron gas systems. The strong density modulations in these systems were one dimensional and periodic, with roughly sinusoidal profiles. The simplicity of the density profiles allowed us to perform a detailed analysis of the effect of inhomogeneity on the behavior of n_{xc}, g_{xc}, and e_{xc}, and the performance of various approximations to these quantities.

The ISI model for W_{xc}^{λ}, combined with the gradient-corrected PC approximation for the strong interaction limit, was found to describe the adiabatic VMC curves with remarkable accuracy in our systems. The pair-correlation functions were stretched in the direction of the inhomogeneity and had a strongly asymmetric shape in regions of high density gradient. This behavior, together with the strong variation of $n(\mathbf{r})$ on the scale of the inverse local Fermi wave vector $k_F(\mathbf{r})^{-1} = (3\pi^2 n(\mathbf{r}))^{-1/3}$, resulted in a strikingly nonlocal behavior of n_{xc}. Our examination of the second-order GEA showed that it was unable to capture the strongly nonlocal behavior of the exchange hole around the density minima; it was also unable to describe the energetically important contraction of the exchange hole in the direction of the inhomogeneity at the density maxima.

The LDA errors in e_{xc} were found to have a dominant and energetically significant component, the magnitude, shape, and sign of which are controlled by the semilocal quantity $\nabla^2 n(\mathbf{r})$. Because it depends only on n and $|\nabla n|$, the GGA is unable to correct the LDA errors in E_{xc} resulting from this component adequately, and worsens the LDA in two of our three systems. When the LDA errors in the exchange and correlation contributions to e_{xc} were considered separately, it was found that the Laplacian component is mainly due to exchange. The point-wise cancellation between the LDA errors in e_x and e_c was found to be effective for the system with the slowest density modulations, but became less effective in the other two systems. In particular, we found a conspiracy of the LDA errors in e_x and e_c occurring in the regions around density maxima.

One of the problems with current GGA and meta-GGA functionals is that their improvement upon the LDA is system dependent. Our investigations have shed new light on the reasons behind this inconsistent behavior. In particular, we have seen that the GGA will always fail to describe systems in which the LDA overestimation of e_{xc} around density maxima dominates the underestimation of this quantity elsewhere. Current GGA functionals are constructed such that their exchange enhancement factor $F_x^{GGA}(s)$ is always greater than or equal to unity. To improve upon the LDA in systems such as ours, however, it is clear that F_x must be allowed to take on values smaller than unity (exchange de-enhancement). This cannot be achieved with the limited functional form $F_x^{GGA}(s)$.

Taken as a whole, our results suggest that accurate enhancement factors are likely to depend on both s and l (at least). In order to find a "universal" form, one would have to evaluate F_x for many different systems, each representing a different class of electron densities. In this way, a complete "scatter map" of F_x against $(s, l, \ldots)$ could be obtained (within the physically relevant ranges of these parameters). The scatter map could then be used to find an energetically accurate fit of F_x as a function of the chosen set of parameters. We note that a recent numerical study of the analytical structure of the exchange energy per electron[44], performed for the so-called Matthieu gas, suggests that the Laplacian coefficient in an expansion of the form

$$e_x(\mathbf{r}, [n]) = e_x^{LDA}(1 + as^2 + bl + \ldots) \qquad (55)$$

is not well-defined. This indicates that such an expansion would not be a suitable starting point for fitting the above-mentioned scatter maps of F_x.

Our work has made available the key quantities in density functional theory for a few relatively simple but strongly inhomogeneous systems. We hope that the simplicity of these systems will encourage the use of our data in the design and testing of new functionals. Since we provide results for both integrated and local quantities, tests of new functionals can now be made on a point-by-point basis.

Our variational Monte Carlo approach based on accurate many-electron wavefunctions provides a computationally affordable methodology for extracting the main point-wise quantities that must be approximated in density-functional calculations of extended systems. To investigate the performance of current approximate functionals more fully, and to guide the construction of better functionals, it would be useful to carry out similar calculations for many other systems, including surfaces and the quasi-two-dimensional electron gas. The techniques developed here may also be extended to investigate spin-polarized DFT.[45]

ACKNOWLEDGMENTS

We thank Stefan Kurth for useful discussions regarding the ISI model, John Perdew for helpful comments on the GEA exchange hole, and Lorna Smith of the Edinburgh Parallel Computing Centre (EPCC) for help with the visualization. Our simulations were performed on the CRAY-T3E at EPCC.

APPENDIX A

We consider a uniform electron gas consisting of N electrons in a simulation cell. We require that the corresponding ground-state wavefunction satisfies periodic

boundary conditions within this cell. For simplicity, we assume that the simulation cell is a cube with side L and volume $\Omega = L^3$. Our results, however, are equally valid for other periodic simulation cells. The electron density of this system is $n = N/L^3$, corresponding to $r_s = (3/4\pi)^{1/3} N^{-1/3} L$. The electron-electron interaction $V_{ee}^L(\mathbf{r})$ we consider is either the standard periodic Ewald interaction or the interaction given by Eq. (26). In both cases it can be shown that $V_{ee}^L(\mathbf{r})$ satisfies the scaling relation

$$V_{ee}^L(\mathbf{r}) = \alpha V_{ee}^{\alpha L}(\alpha \mathbf{r}) \,, \tag{56}$$

where $\mathbf{r}$ is any point in the simulation cell of side L and $V_{ee}^{\alpha L}$ is the electron-electron interaction associated with a simulation cell of side αL. The many-body wavefunction Ψ_L^λ for a simulation cell of side L containing N electrons interacting with coupling constant λ satisfies

$$\left[\sum_{i=1}^{N} -\frac{1}{2}\nabla_i^2 + \lambda \sum_{i>j} V_{ee}^L(\mathbf{r}_{ij})\right] \Psi_L^\lambda(\mathbf{r}_1, \ldots, \mathbf{r}_N) = E_L^\lambda \Psi_L^\lambda(\mathbf{r}_1, \ldots, \mathbf{r}_N) \,, \tag{57}$$

where the points $\mathbf{r}_i$, $i = 1, \ldots, N$, all lie in the simulation cell of side L. Using the scaling relation with $\alpha = \lambda$, this becomes

$$\left[\sum_{i=1}^{N} -\frac{1}{2}\nabla_i^2 + \lambda^2 \sum_{i>j} V_{ee}^{\lambda L}(\lambda \mathbf{r}_{ij})\right] \Psi_L^\lambda(\mathbf{r}_1, \ldots, \mathbf{r}_N) = E_L^\lambda \Psi_L^\lambda(\mathbf{r}_1, \ldots, \mathbf{r}_N) \,, \tag{58}$$

and thus, making the substitution $\mathbf{r}_i' = \lambda \mathbf{r}_i$, we obtain:

$$\left[\sum_{i=1}^{N} -\frac{1}{2}\nabla_{i'}^2 + \sum_{i>j} V_{ee}^{\lambda L}(\mathbf{r}_{ij}')\right] \Psi_L^\lambda(\mathbf{r}_1'/\lambda, \ldots, \mathbf{r}_N'/\lambda) = \frac{E_L^\lambda}{\lambda^2} \Psi_L^\lambda(\mathbf{r}_1'/\lambda, \ldots, \mathbf{r}_N'/\lambda) \,. \tag{59}$$

This shows that $\Psi_L^\lambda(\mathbf{r}_1'/\lambda, \ldots, \mathbf{r}_N'/\lambda)$ is proportional to the ground-state wavefunction $\Psi_{\lambda L}^{\lambda=1}(\mathbf{r}_1', \ldots, \mathbf{r}_N')$ of a system of N electrons interacting at full ($\lambda = 1$) coupling and satisfying periodic boundary conditions in a simulation cell of side λL:

$$\Psi_L^\lambda(\mathbf{r}_1'/\lambda, \ldots, \mathbf{r}_N'/\lambda) = C^\lambda \Psi_{\lambda L}^{\lambda=1}(\mathbf{r}_1', \ldots, \mathbf{r}_N') \,. \tag{60}$$

The electron density in the simulation cell of side λL corresponds to $r_s' = \lambda r_s$ and thus

$$\Psi_{r_s}^\lambda(\mathbf{r}_1'/\lambda, \ldots, \mathbf{r}_N'/\lambda) = C^\lambda \Psi_{\lambda r_s}^{\lambda=1}(\mathbf{r}_1', \ldots, \mathbf{r}_N') \,. \tag{61}$$

When re-expressed in terms of $\mathbf{r}_i = \mathbf{r}_i'/\lambda$, this becomes:

$$\Psi_{r_s}^\lambda(\mathbf{r}_1, \ldots, \mathbf{r}_N) = C^\lambda \Psi_{\lambda r_s}^{\lambda=1}(\lambda \mathbf{r}_1, \ldots, \lambda \mathbf{r}_N) \,. \tag{62}$$

APPENDIX B

Symmetry considerations require that the exchange energy density at $\mathbf{r}$ must be a function of $n(\mathbf{r})$ and its rotationally invariant derivatives such as $|\nabla n(\mathbf{r})|$ and $\nabla^2 n(\mathbf{r})$. This ensures that all rotations of the entire density about the point $\mathbf{r}$ leave the value of $e_{xc}(\mathbf{r})$ invariant. We thus write

$$\begin{aligned} E_x[n] &= \int d\mathbf{r}\; e_x^{LDA}(n(\mathbf{r}))\, F_x(n(\mathbf{r}), |\nabla n(\mathbf{r})|, \nabla^2 n(\mathbf{r}), \ldots) \\ &= C_x \int d\mathbf{r}\; n^{4/3}(\mathbf{r})\, F_x(n(\mathbf{r}), |\nabla n(\mathbf{r})|, \nabla^2 n(\mathbf{r}), \ldots) \,, \end{aligned} \tag{63}$$

where $C_x = -3(3\pi^2)^{1/3}/4\pi$. Substitution of $n_\gamma(\mathbf{r}) = \gamma^3 n(\gamma \mathbf{r})$ into the above equation yields:

$$\begin{aligned} E_x[n_\gamma] \;=\; & C_x \int d\mathbf{r}\; \gamma^4 n^{4/3}(\gamma \mathbf{r}) \\ & \times\; F_x(\gamma^3 n(\gamma \mathbf{r}), |\nabla(\gamma^3 n(\gamma \mathbf{r}))|, \nabla^2(\gamma^3 n(\gamma \mathbf{r})), \ldots) \,, \end{aligned} \tag{64}$$

or, putting $\mathbf{r}' = \gamma \mathbf{r}$,

$$\begin{aligned} E_x[n_\gamma] \;=\; & \gamma C_x \int d\mathbf{r}'\; n^{4/3}(\mathbf{r}') \\ & \times F_x(\gamma^3 n(\mathbf{r}'), \gamma |\nabla'(\gamma^3 n(\mathbf{r}'))|, \gamma^2 \nabla'^2(\gamma^3 n(\mathbf{r}')), \ldots) \,. \end{aligned} \tag{65}$$

Finally, relabeling $\mathbf{r}'$ as $\mathbf{r}$, we obtain

$$\begin{aligned} E_x[n_\gamma] \;=\; & \gamma C_x \int d\mathbf{r}\; n^{4/3}(\mathbf{r}) \\ & \times\; F_x(\gamma^3 n(\mathbf{r}), \gamma^4 |\nabla n(\mathbf{r})|, \gamma^5 \nabla^2 n(\mathbf{r}), \ldots) \,. \end{aligned} \tag{66}$$

The homogeneous scaling property of E_x, Eq. (52), then requires that

$$\begin{aligned} & \gamma C_x \int d\mathbf{r}\; n^{4/3}(\mathbf{r})\, F_x(\gamma^3 n(\mathbf{r}), \gamma^4 |\nabla n(\mathbf{r})|, \gamma^5 \nabla^2 n(\mathbf{r}), \ldots) \\ & = \gamma C_x \int d\mathbf{r}\; n^{4/3}(\mathbf{r})\, F_x(n(\mathbf{r}), \nabla n(\mathbf{r}), \nabla^2 n(\mathbf{r}), \ldots) \end{aligned} \tag{67}$$

for any arbitrary scaling factor $\gamma > 0$. This condition is fulfilled for an arbitrary v-representable density if and only if the enhancement factor satisfies the equation:

$$\begin{aligned} & F_x(\gamma^3 n(\mathbf{r}), \gamma^4 |\nabla n(\mathbf{r})|, \gamma^5 \nabla^2 n(\mathbf{r}), \ldots) \\ & \quad = \; F_x(n(\mathbf{r}), \nabla n(\mathbf{r}), \nabla^2 n(\mathbf{r}), \ldots) \,. \end{aligned} \tag{68}$$

Furthermore, when all gradients are zero, we should, of course, have $F_x = 1$. Both requirements may be fulfilled simultaneously by choosing F_x to be of the following form:

$$F_x = F_x\left(\frac{|\nabla n(\mathbf{r})|}{n^{4/3}(\mathbf{r})}, \frac{\nabla^2 n(\mathbf{r})}{n^{5/3}(\mathbf{r})}, \ldots\right) \,, \tag{69}$$

which may also be written in terms of the reduced gradient $s(\mathbf{r}) = |\nabla n(\mathbf{r})|/(2k_F(\mathbf{r})n(\mathbf{r}))$, the reduced Laplacian $l(\mathbf{r}) = \nabla^2 n(\mathbf{r})/(4k_F^2(\mathbf{r})n(\mathbf{r}))$, and so on.

[*] W. M. C. Foulkes acknowledges the hospitality of the Kavli Institute for Theoretical Physics, University of California, Santa Barbara, where some amendments to this paper were completed during a visit to the Research Program on Realistic Theories of Correlated Electron Materials.

[1] P. Hohenberg and W. Kohn, Phys. Rev. **136**, B864 (1964).
[2] W. Kohn, Nobel Lecture, Rev. Mod. Phys. **71**, 1253 (1998).
[3] W. Kohn and L. J. Sham, Phys. Rev. **140**, A1133 (1965).
[4] J. P. Perdew, K. Burke, and M. Ernzerhof, Phys. Rev. Lett. **77**, 3865 (1996).
[5] J. P. Perdew and Y. Wang, Phys. Rev. B **33**, 8800 (1986).
[6] A. D. Becke, Phys. Rev. A **38**, 3098 (1988); A. D. Becke, J. Chem. Phys. **98**, 5648 (1993).
[7] C. Lee, W. Yang, and R. G. Parr, Phys. Rev. B **37**, 785 (1988).
[8] See, e.g., J. P. Perdew, S. Kurth, A. Zupan, and P. Blaha, Phys. Rev. Lett. **82**, 2544 (1999).
[9] O. Gunnarsson, M. Jonson, and B. I. Lundqvist, Phys. Rev. B **20**, 3136 (1979).
[10] A. D. Becke, J. Chem. Phys. **98**, 1372 (1993).
[11] An alternative to the wavefunction approach is to obtain n_{xc}^{λ} via the fluctuation-dissipation theorem from the dynamic density-density response function associated with coupling λ. The response function could be obtained, e.g., from many-body perturbation theory.
[12] D. Joubert and G. P. Srivastava, J. Chem. Phys. **109**, 5212 (1998).
[13] F. Colonna and A. Savin, J. Chem. Phys. **110**, 2828 (1999).
[14] B. L. Hammond, W. A. Lester, Jr., and P. J. Reynolds, *Monte Carlo Methods in Ab Initio Quantum Chemistry* (World Scientific, Singapore, 1994).
[15] For a recent review see W. M. C. Foulkes, L. Mitas, R. J. Needs, and G. Rajagopal, Rev. Mod. Phys. **73**, 33 (2001).
[16] M. Nekovee, W. M. C. Foulkes, A. J. Williamson, G. Rajagopal, and R. J. Needs, Adv. Quantum Chem. **33**, 189 (1999).
[17] M. Nekovee, W. M. C. Foulkes, and R. J. Needs, Phys. Rev. Lett. **87**, 036401 (2001).
[18] R. G. Parr and W. Yang, *Density Functional Theory of Atoms and Molecules* (Oxford University Press, Oxford, 1988).
[19] C. J. Umrigar, K. G. Wilson, and J. W. Wilkins, Phys. Rev. Lett. **60**, 1719 (1988).
[20] A. J. Williamson, S. D. Kenny, G. Rajagopal, A. James, R. J. Needs, L. M. Fraser, W. M. C. Foulkes, and P. Maccallum, Phys. Rev. B **53**, 9640 (1996).
[21] R. Q. Hood, M. Y. Chou, A. J. Williamson, G. Rajagopal, R. J. Needs, and W. M. C. Foulkes, Phys. Rev. Lett. **78**, 3350 (1997); Phys. Rev. B **57**, 8972 (1998).
[22] The minimization was carried out using the combined Gauss-Newton and modified Newton method implemented in subroutine E04FCF from the NAG Fortran Library, `www.nag.co.uk/numeric/FL/FLdescription.asp`.
[23] The integration was carried out using the Gill-Miller quadrature method implemented by subroutine D01GAF from the NAG Fortran Library, `www.nag.co.uk/numeric/FL/FLdescription.asp`.
[24] R. Gaudoin, M. Nekovee, W. M. C. Foulkes, R. J. Needs and G. Rajagopal, Phys. Rev. B **63**, 115115 (2001).
[25] See S. Fahy, X. W. Wang, and S. G. Louie, Phys. Rev. Lett. **61**, 1631 (1998).
[26] A. J. Williamson, G. Rajagopal, R. J. Needs, L. M. Fraser, W. M. C. Foulkes, Y. Wang, M. Y. Chou, Phys. Rev. B **55**, R4851 (1997); L. M. Fraser, W. M. C. Foulkes, G. Rajagopal, R. J. Needs, S. D. Kenny, and A. J. Williamson, *ibid.* **53**, 1814 (1996).
[27] J. P. Perdew and A. Zunger, Phys. Rev. B **23**, 5048 (1981).
[28] A. Görling and M. Levy, Phys. Rev. B **47**, 13105 (1993).
[29] A. Savin, Phys. Rev. A **52**, R1805 (1995).
[30] M. Ernzerhof, Chem. Phys. Lett. **263**, 1996.
[31] M. Seidl, J. P. Perdew, and M. Levy, Phys. Rev. A **59**, 51 (1999).
[32] M. Seidl, J. P. Perdew, and S. Kurth, Phys. Rev. A **62**, 012502 (2000).
[33] M. Seidl, J. P. Perdew, and S. Kurth, Phys. Rev. Lett. **84**, 5070 (2000).
[34] We thank the anonymous referee for bringing this point to our attention.
[35] M. Nekovee and J. M. Pitarke, Comp. Phys. Comm. **137**, 123 (2001).
[36] Y.-H. Kim *et al.*, Phys. Rev. B **61**, 5202 (2000); L. Pollack and J. P. Perdew, J. Phys.: Cond. Matt. **7**, 1239 (1999).
[37] W. Kohn and A. E. Mattsson, Phys. Rev. Lett. **81**, 3487 (1998).
[38] P. P. Rushton, D. J. Tozer, and S. J. Clark, Phys. Rev. B **65**, 193106 (2002).
[39] E. K. U. Gross and R. M. Dreizler, Z. Phys. A **302**, 103 (1981).
[40] J. P. Perdew, Phys. Rev. Lett. **55**, 1665 (1985).
[41] A. Puzder, M. Y. Chou, and R. Q. Hood, Phys. Rev. A **64**, 022501 (2001).
[42] P. R. T. Schipper, O. V. Gritsenko, and E. J. Baerends, Phys. Rev. A **57**, 1729 (1998).
[43] M. Levy and J. P. Perdew, Phys. Rev. A **32**, 2010 (1985).
[44] R. Armiento and A. E. Mattsson, Phys. Rev. B **66**, 165117 (2002).
[45] M. Nekovee (unpublished).

TABLE I: Exchange energies (Hartrees per electron) and the LDA and GGA exchange-energy errors, $\Delta E_x^{LDA} = E_x^{LDA} - E_x^{VMC}$ and $\Delta E_x^{GGA} = E_x^{GGA} - E_x^{VMC}$, for the three different values of the wave vector q.

q/k_F^0	E_x^{VMC}	ΔE_x^{LDA}	ΔE_x^{GGA}
1.11	−0.2930	+0.0111	−0.0037
1.55	−0.2756	+0.0046	−0.0161
2.17	−0.2534	+0.0000	−0.0228

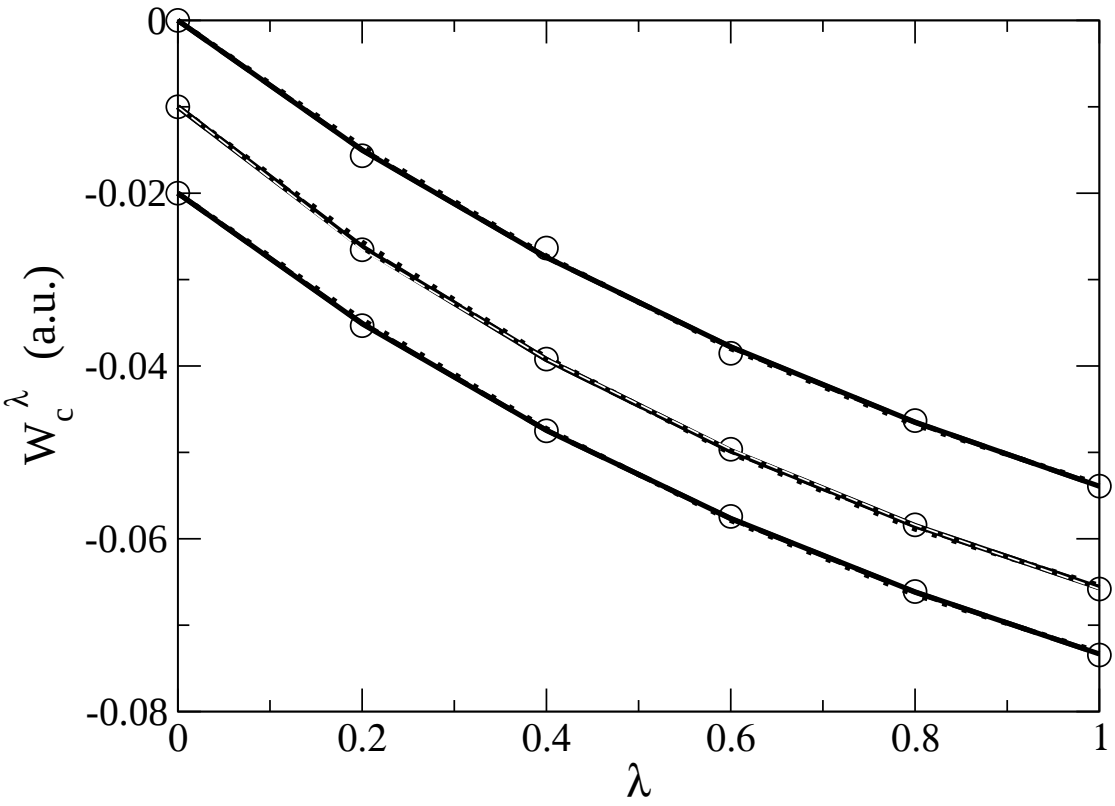

FIG. 1: The VMC results (circles) for W_c^λ in the $q = 1.1080k_F^0$, $q = 1.556k_F^0$, and $q = 2.172k_F^0$ systems. The curves corresponding to the $q = 1.556k_F^0$ and $q = 2.172K_F^0$ systems have been offset, respectively, by -0.01 and -0.02 a.u. along the y axis. Also shown are the corresponding quadratic (dotted lines), Padé (solid lines), and Yukawa (dashed lines) fits.

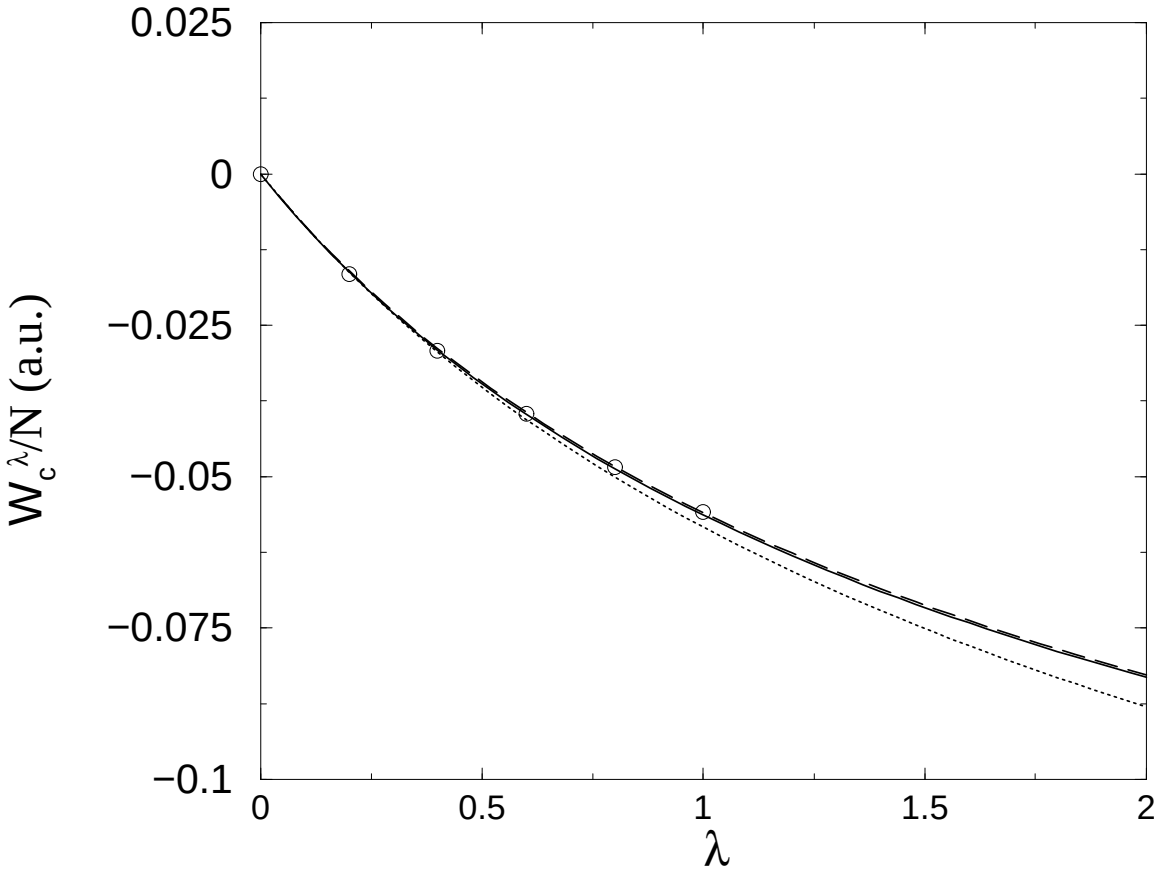

FIG. 2: The VMC results (circles) for W_c^{λ} in the range $0 \leq \lambda \leq 1$ are compared with the curves obtained from the ISI-PC model for the $q = 1.556k_F^0$ system in the range $0 \leq \lambda \leq 2$. The ISI-PC curves were computed using the values of $W_c'^{,0}$ obtained from the Padé (solid line) and Yukawa (dashed line) fits to the VMC data combined with the gradient-corrected PC model for W_c^{∞} and $W_c'^{,\infty}$. The ISI-PC curve obtained without the inclusion of gradient terms is also shown (dotted line).

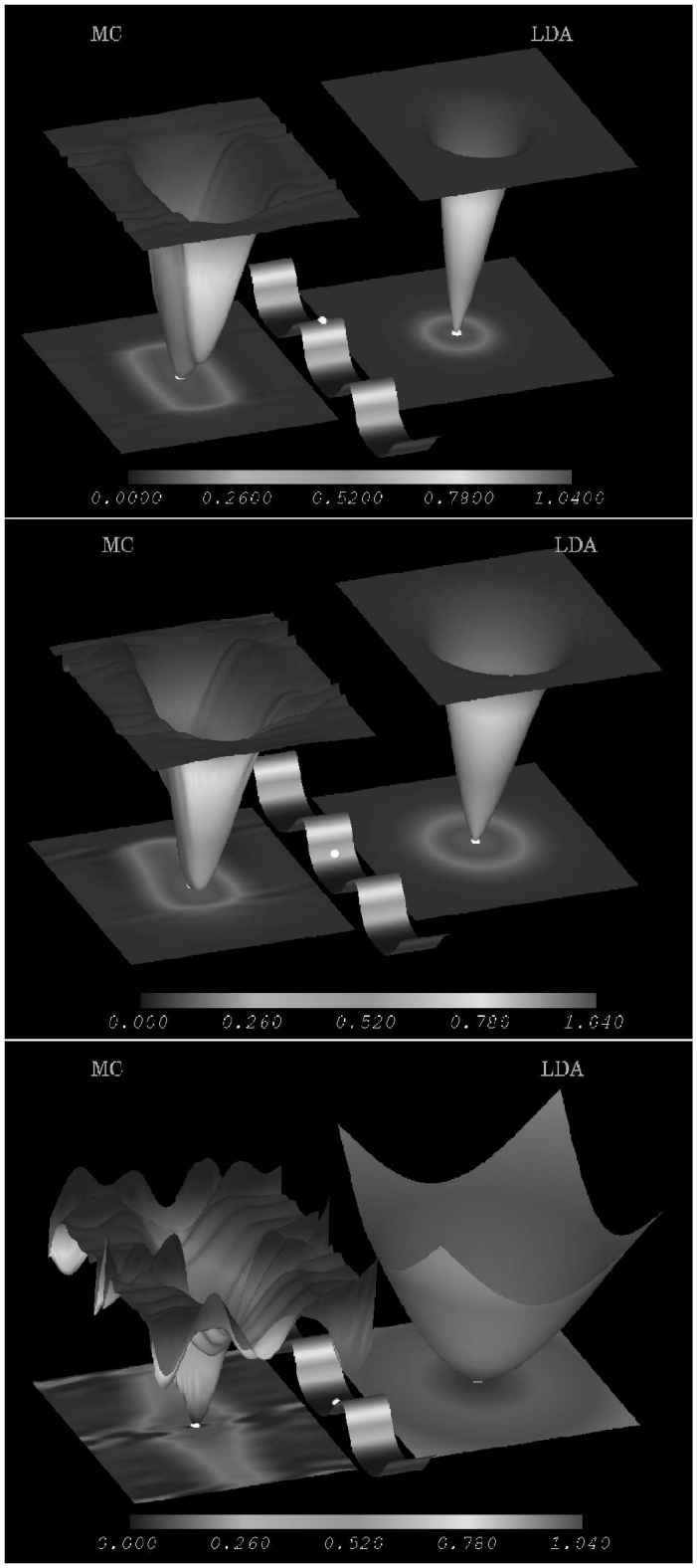

FIG. 3: The VMC and LDA pair-correlation functions, $g_{xc}(\mathbf{r}, \mathbf{r}')$, for the strongly inhomogeneous $q = 1.1080k_F^0$ system. The pair-correlation function is plotted for $\mathbf{r}$ at a density maximum (top), on the slope (middle), and at a density minimum (bottom), with $\mathbf{r}'$ ranging in a plane parallel to $\mathbf{q}$ (the direction of maximum inhomogeneity). The electron density is shown schematically, with the point $\mathbf{r}$ indicated by a white bullet.

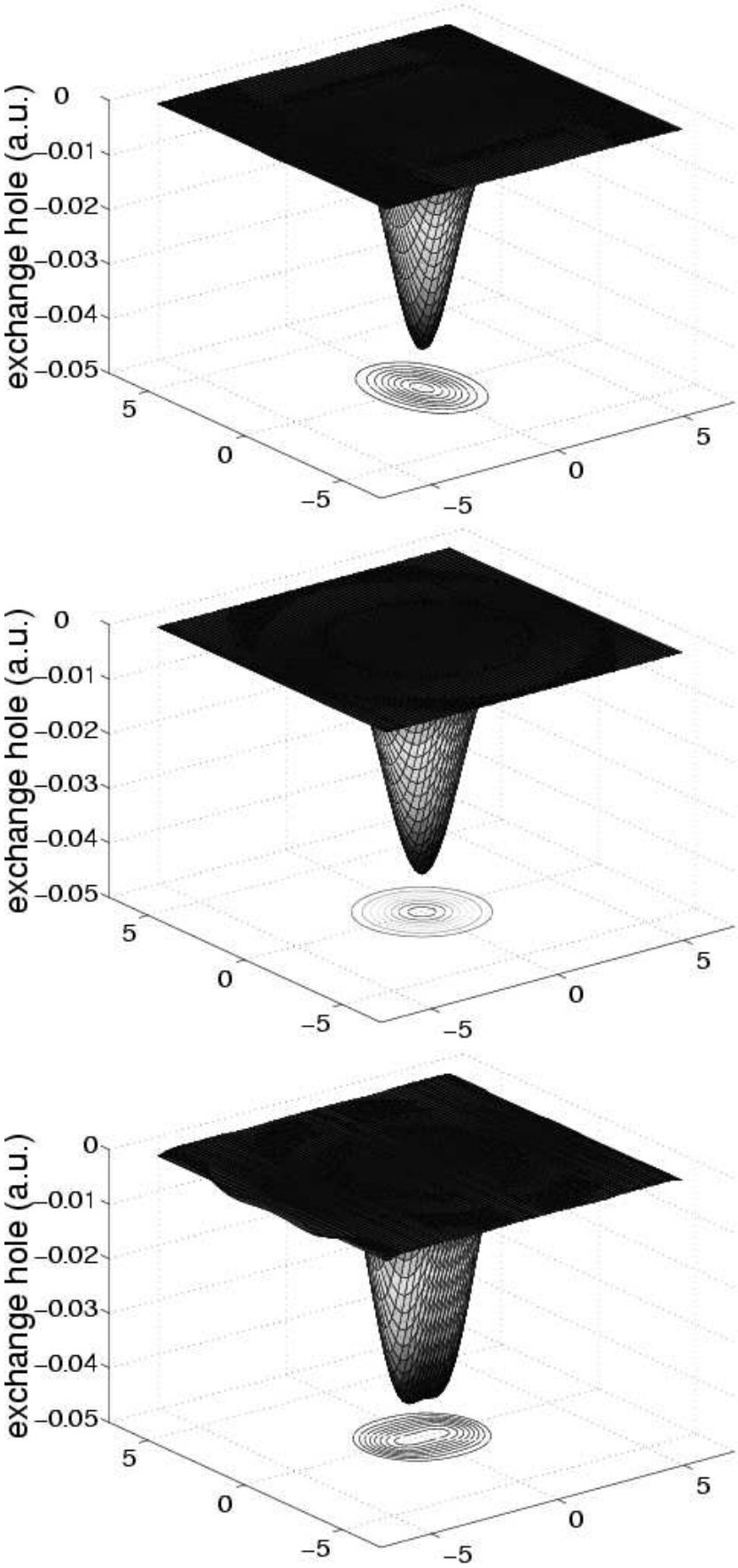

FIG. 4: The exact, LDA and truncated GEA exchange holes, $n_x(\mathbf{r}, \mathbf{r}+\mathbf{R})$, for the strongly inhomogeneous $q = 1.1080k_F^0$ system plotted for $\mathbf{r}$ at a density maximum and $\mathbf{R}$ ranging in a plane parallel to $\mathbf{q}$. Distances are in atomic units.

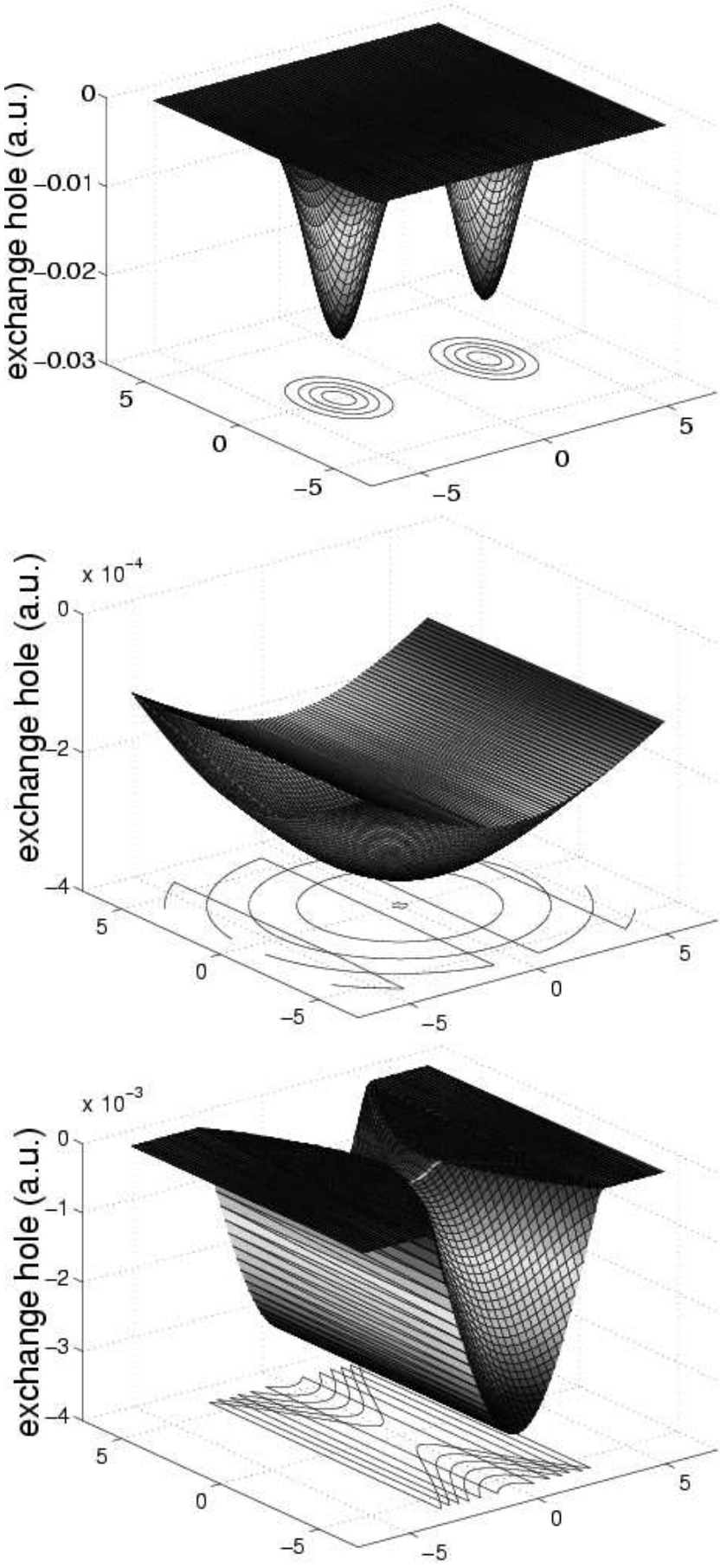

FIG. 5: The exact, LDA and truncated GEA exchange holes, $n_x(\mathbf{r}, \mathbf{r}+\mathbf{R})$, for the strongly inhomogeneous $q = 1.1080k_F^0$ system plotted for $\mathbf{r}$ at a density minimum and $\mathbf{R}$ ranging in a plane parallel to $\mathbf{q}$. Distances are in atomic units.

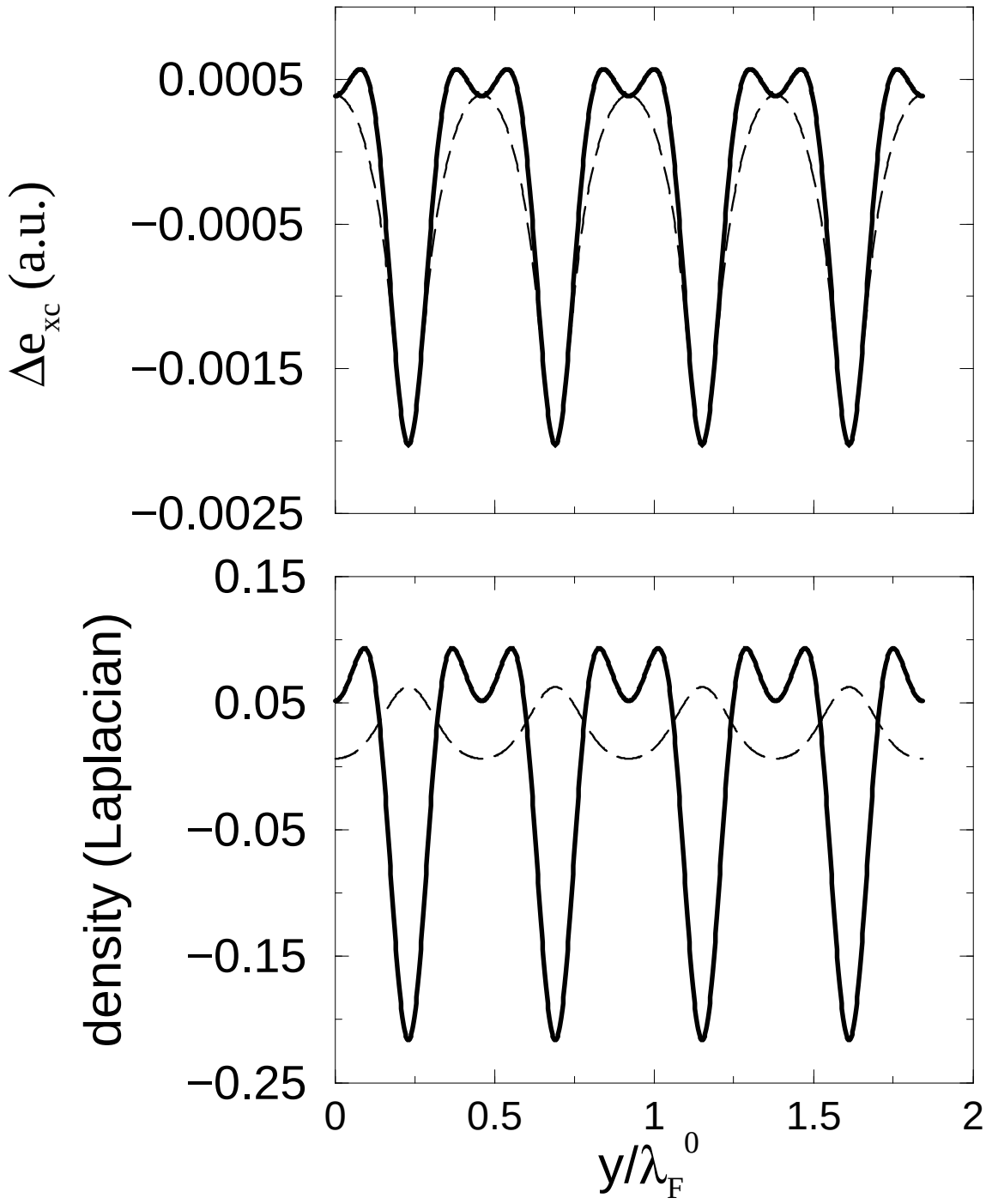

FIG. 6: The upper graph shows $e_{xc}^{LDA} - e_{xc}^{VMC}$ (heavy line) and $e_{xc}^{GGA} - e_{xc}^{VMC}$ (light line) along a direction parallel to $\mathbf{q}$ (we call this y) for the $q = 2.172k_F^0$ system. The lower graph shows the corresponding electron density (light line) and Laplacian (heavy line). Distances are in units of the Fermi wavelength $\lambda_F^0 = 2\pi/k_F^0$ corresponding to the average density.

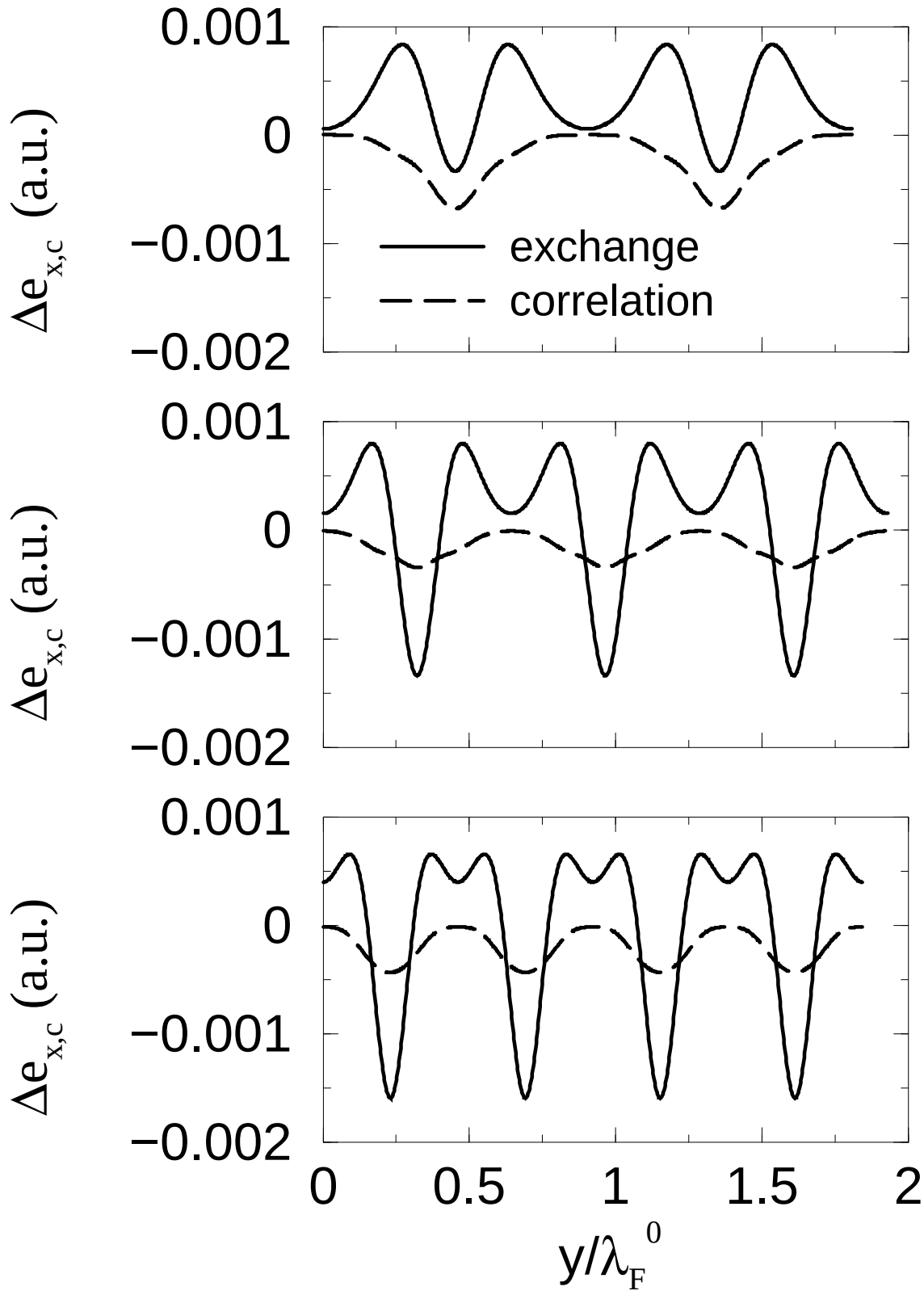

FIG. 7: The differences $e_x^{LDA} - e_x^{VMC}$ (solid lines) and $e_c^{LDA} - e_c^{VMC}$ (dashed lines) are shown along a direction parallel to **q** for (from top to bottom) the $q = 1.1080k_F^0$, $q = 1.556k_F^0$, and $q = 2.172k_F^0$ systems.

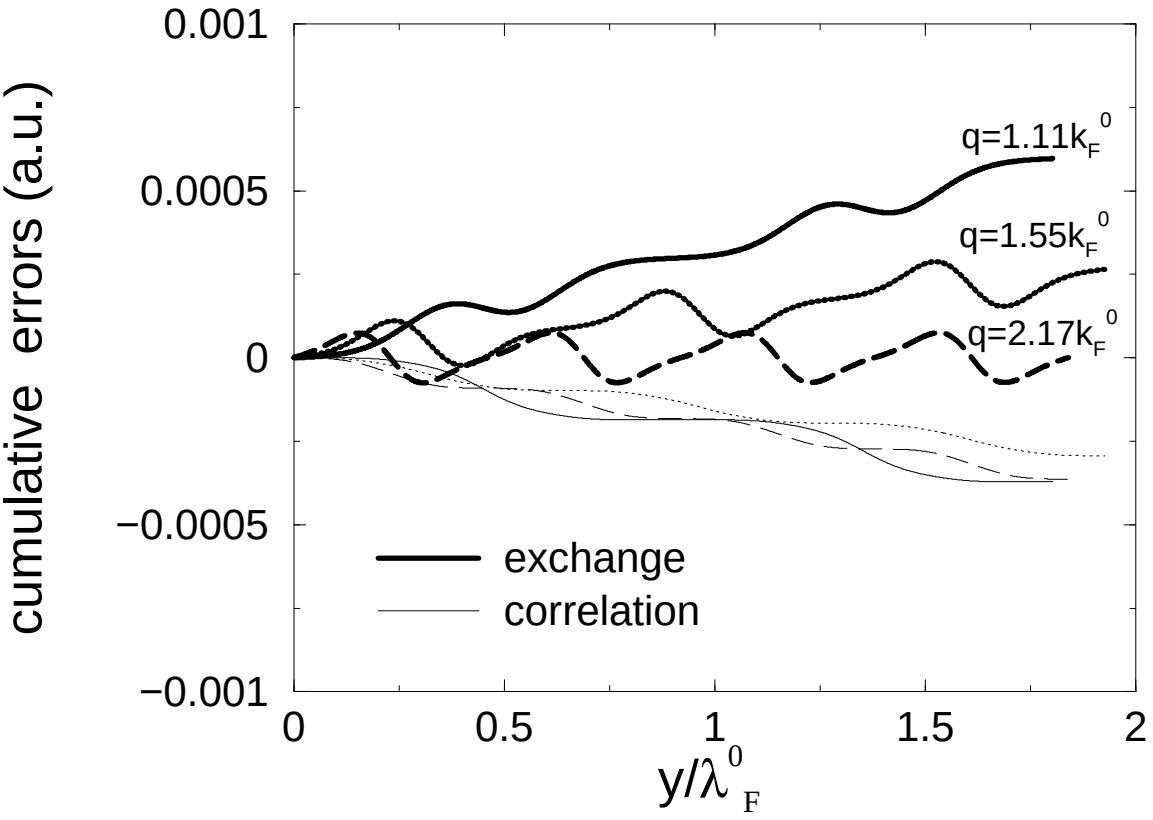

FIG. 8: The cumulative LDA errors in the exchange (the three upper curves) and correlation (the three lower curves) energy densities as functions of y.

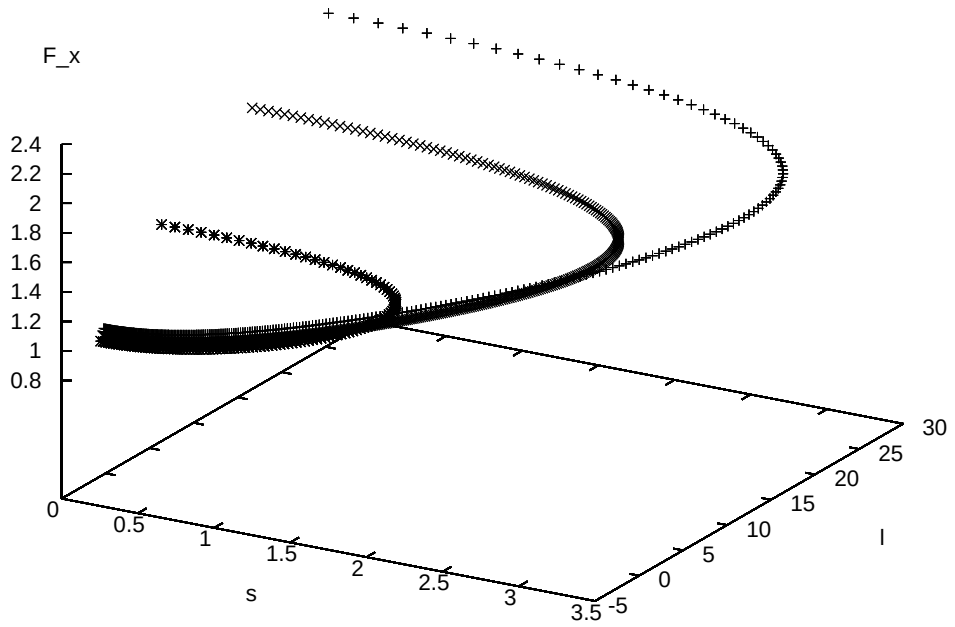

FIG. 9: The values of the exact enhancement factor F_x are plotted against the values of the reduced density gradient s and the reduced Laplacian l for the $q = 1.1080k_F^0$ system (plus signs), the $q = 1.556k_F^0$ system (crosses), and the $q = 2.172k_F^0$ system (stars).